Energy Conversion and Management 182 (2019) 412–429

Contents lists available at ScienceDirect

Energy Conversion and Management

journal homepage: www.elsevier.com/locate/enconman

Multi-objective optimization of sorption enhanced steam biomass gasification with solid oxide fuel cell

Thanaphorn Detchusananard[a], Shivom Sharma[b], François Maréchal[b], Amornchai Arpornwichanop[a,*]

[a] Computational Process Engineering Research Unit, Department of Chemical Engineering, Faculty of Engineering, Chulalongkorn University, Bangkok 10330, Thailand
[b] Industrial Process and Energy Systems Engineering, École Polytechnique Fédérale de Lausanne, EPFL, CH-1951 Sion, Switzerland

ARTICLE INFO

Keywords:
Steam gasification
CO_2 capture
Sorption enhanced steam biomass gasification
Solid oxide fuel cell
Exergy analysis
Multi-objective optimization

ABSTRACT

Biomass is one of the encouraging renewable energy sources to mitigate uncertainties in the future energy supply and to address the climate change caused by the increased CO_2 emissions. Conventionally, thermal energy is produced from biomass via combustion process with low thermodynamic efficiency. Conversely, gasification of biomass integrated with innovative power generation technologies, such as Solid Oxide Fuel Cell (SOFC), offers much higher conversion efficiency. Typically, energy conversion process has multiple conflicting performance criteria, such as capital and operating costs, annual profit, thermodynamic performance and environment impact. Multi-objective Optimization (MOO) methods are used to found the optimal compromise in the objective function space, and also to acquire the corresponding optimal values of decision variables. This work investigates integration and optimization of a Sorption Enhanced Steam Biomass Gasification (SEG) with a SOFC and Gas Turbine (GT) system for the production of power and heat from Eucalyptus wood chips. The energy system model is firstly developed in Aspen Plus simulator, which has five main units: (1) SEG coupled with calcium looping for hydrogen-rich gas production, (2) hot gas cleaning and steam reforming, (3) SOFC-GT for converting hydrogen into electricity, (4) catalytic burning and CO_2 compression, and (5) cement production from the purge CaO stream of SEG unit. Then, the design and operating variables of the conversion system are optimized for annual profit, annualized total capital cost, operating cost and exergy efficiency, using MOO. Finally, for the implementation purpose, two selection methods and parametric uncertainty analysis are performed to identify good solutions from the Pareto-optimal front.

1. Introduction

The increase in energy demand and global warming concern worldwide have driven the research and development of innovative power production technology with high conversion efficiency and low carbon footprint. Additionally, fossil fuels including coal, natural gas and petroleum are finite and non-renewable, and their use in the combustion engines to produce power and electricity increases the pollution levels in the environment. Therefore, many researchers are focusing on the development of advanced power generation technologies with high efficiencies and low CO_2 emissions. Biomass is assumed to be an attractive feedstock for power and heat generations, as it is renewable and widely-available resource, and might be produced sustainably in the future [1,2].

Biomass feedstock can be used for both heat and power generations through biochemical and thermochemical processes [3]. The biochemical processes, such as anaerobic digestion and fermentation, involve use of enzymes, microorganisms and bacteria to breakdown biomass into liquid (e.g., bioethanol) and gaseous fuels (e.g., biogas). Conversely, thermochemical processes such as combustion, pyrolysis and gasification involve the use of heat as primary mechanism for converting biomass into hydrocarbons [4]. Among these processes, gasification has a lower emission of pollutants and higher efficiency of power and heat generations [5]. In biomass gasification, biomass is converted into a combustible or synthesis gas (syngas) which contains mainly methane, hydrogen, carbon monoxide and carbon dioxide. Gasification occurs when a gasifying agent (steam, oxygen, air, or mixture of gasifying agents) is reacted with the available carbon in biomass inside a gasifier at high temperature. Gasification of biomass with air produces low quality syngas (higher heating value = 4–7 MJ m^{-3}), whereas use of steam or oxygen as a gasifying agent gives high quality syngas (higher heating value = 10–18 MJ m^{-3}). However, gasification

* Corresponding author.
E-mail address: Amornchai.A@chula.ac.th (A. Arpornwichanop).

https://doi.org/10.1016/j.enconman.2018.12.047
Received 8 September 2018; Accepted 16 December 2018
Available online 06 January 2019
0196-8904/

Nomenclature

A	area (cm^{-2})
C	mass fraction of carbon (–)
E_A	activation energy of the exchange current density (J mol^{-1})
ex	specific exergy transfer with molar flow (kJ $kmol^{-1}$)
$\dot{E}n$	energy rate (kJ h^{-1})
$\dot{E}x$	exergy rate (kJ h^{-1})
F	Faraday's constant (C mol^{-1})
f_{CC}	current collection correction factor (–)
$\dot{G}$	available Gibbs free enthalpy flow (kJ h^{-1})
h	specific enthalpy (kJ $kmol^{-1}$)
H	mass fraction of hydrogen (–)
I	current (A)
J	current density (A cm^{-2})
L	thickness (cm)
LHV	lower heating value (kJ kg^{-1})
$\dot{M}$	mass flow rate (kg h^{-1})
$\dot{n}$	molar flow rate (kmol h^{-1})
N	mass fraction of nitrogen (–) or numbers of cell
O	mass fraction of oxygen (–)
P	preference threshold (–)
Q	indifference threshold (–)
$\dot{Q}$	heat rate (kJ h^{-1})
R	molar gas constant (J mol^{-1} K^{-1}) or specific resistance (Ω cm^2)
s	specific entropy (kJ $kmol^{-1}$ K^{-1})
T	temperature (K) or SOFC operating temperature (K)
U_f	fuel utilization (–)
V	veto threshold (–)
W	weightage (–)
$\dot{W}$	mechanical work rate or electricity production (kJ h^{-1})
y	mole fraction (–)
ΔH°_{298}	heat of reaction at 1 atm and 298.15 K (kJ $kmol^{-1}$)

Greek symbols

β	correlation factor (–)
η	efficiency (%) or loss (V)
λ	air excess (–)
σ	electronic conductivity of electrode or ionic conductivity of electrolyte (S cm^{-1})

Subscripts

0	environmental state at 1 atm and 298.15 K
a	anode side
act	activation
biomass	biomass
c	cathode side
ch	chemical
com	combustion
des	destruction
diff	polarization
E	electrode
EX	exergy
I	interconnect
i	stream i
in	inlet stream
j	component j, objective function j
ohm	ohmic
out	outlet stream
ph	physical
ref	reforming
reg	regeneration

with oxygen has not been applied for biomass because of the higher cost of oxygen production using current commercial technology (e.g., cryogenic air separation) [4]. Steam biomass gasification coupled with calcium looping, called as Sorption Enhanced Steam Biomass Gasification (SEG), is an innovative technology for hydrogen-rich gas production [6–8]. In gasification process, CO_2 and tar yields in product gas can be reduced by the use of CaO [9]. Production of hydrogen-rich gas from biomass using gasification with in-situ CO_2 capture and tar reduction (use of CaO chemical looping) has been studied by Udomsirichakorn et al. [10]. They reported that the maximum yield and concentration of H_2 were increased to 451.11 ml $g^{-1}_{biomass}$ and 78 vol%, respectively, with steam to biomass ratio of 3.41 and gasifier temperature of 650 °C. Further, for the same operating point, lowest CO_2 concentration and tar content (4.98 vol% and 2.48 g Nm^{-3}) were reported.

In order to develop advanced power generation technology, biomass gasification can be coupled with high-efficiency power generation units such as Solid Oxide Fuel Cell (SOFC). A SOFC is one of the most promising technologies for electricity generation with higher thermodynamic efficiency compared to the conventional technologies [11,12]. A SOFC directly converts chemical energy into electricity with high efficiency and operates at a very high temperature (~600 to 1000 °C) [11]. Recently, biomass gasification integrated with a SOFC system for power generation has been given significant attention by researchers. Colpen et al. [13] simulated an integrated biomass gasification and SOFC system, and studied the use of gasification agents (steam, oxygen, air) on the system performance. Their system includes biomass gasification, hot gas cleaning and fuel cell. The results show that use of steam inside the gasifier gave maximum electrical efficiency (41.8%), exergy efficiency (39.1%) and power/heat ratio (4.65), but minimum efficiency of fuel utilization (50.8%). For oxygen and air gasification agents, exergy destruction had maximum values inside the gasifier. Bang-Moller et al. [14] investigated an integrated plant, biomass gasification, a SOFC and a micro GT, for the combined power and heat generations. They reported that the optimized plant (production capacity ~ 290 kW_e) has electrical efficiency of 58.2% based on the lower heating value of feedstock. Recalde et al. [15] showed that biomass gasifier integrated with a SOFC is more suitable for energy recovery, than any other process such as biochar production by pyrolysis, with the electrical efficiency of 65% and exergy efficiency of 58%.

Usually, energy conversion process has multiple performance criteria, namely thermodynamic conversion efficiency, capital and operating costs, annual profit and environment impact. Multi-objective Optimization (MOO) method is used to find quantitative trade-offs among the conflicting performance criteria and also to get the optimal values of decision variables. Many researchers have studied trade-offs between two or more objective functions using MOO methods [16,17]. Abdollahi and Meratizaman [18] accomplished the thermodynamic and environmental optimization of a small-scale distributed combined heating, cooling and power generation system (CCHP) using genetic algorithms to find the Pareto-optimal front. Quddus et al. [19] investigated optimization of a SOFC for oxidative coupling of methane, using Non-dominated Sorting Genetic Algorithm with Jumping Genes (NSGA-II-aJG). Modeling and optimization of SOFC has thus become a great tool to understand its performance. The optimization results provided better distributed and wider spread of optimal solutions which helps in running a SOFC at desired optimum. Jokar et al. [20] performed thermodynamic study of a molten carbonate fuel cell and supercritical CO_2 Brayton cycle hybrid system. The multi-objective evolutionary method (NSGA) was used to get the Pareto-optimal front, and

three efficient decision making methods namely Fuzzy, LINMAP and TOPSIS were used to select the best solution from the Pareto-optimal front. Sadeghi et al. [21] investigated a syngas fed SOFC power plant using a downdraft gasifier and performed a multi-objective optimization of maximizing the total exergy efficiency and minimizing the normalized CO_2 emission using genetic algorithms method. The optimization results show that minimization of total product unit cost of system as the only criterion leads to the higher value of normalized CO_2 emission and lower value of system exergy efficiency.

This study investigates the integration and optimization of a SEG, SOFC and GT units, based on several performance criteria, to generate electrical power and heat from Eucalyptus wood chips. The energy system model is developed in Aspen Plus simulator (version 8.8). The integrated SEG-SOFC-GT plant is an attractive choice for heat integration because waste heat released by SOFC at high temperature can be consumed in CaO regeneration. In order to optimize the performance of the proposed integrated energy plant, four relevant bi-objective optimization problems have been investigated: (1) maximization of annual profit, minimization of annualized capital cost (ACC), (2) minimization of ACC, maximization of exergy efficiency, (3) minimization of ACC, minimization of operating cost, and (4) minimization of levelized electricity cost, minimization of ACC per kWh. OSMOSE platform is a computer-aided tool which is developed for the design and integration of industrial processes and energy systems, and is also used to study MOO of the proposed integrated energy plant [23–25].

There are several approaches for choosing one of the optimal solutions found for a MOO problem [26]. For the implementation purpose, the preferred optimal solutions from the Pareto front are chosen by Net Flow Method (NFM) and Gray Relational Analysis (GRA). At the end of this study, market economics and plant operating conditions, namely electricity price, wood price, oxygen price, $CaCO_3$ price, Portland cement price, yearly operation, interest rate, capital cost, and economic life time, are used to study parametric uncertainty analysis of the optimal solution found by OSMOSE. Optimal solutions or plant designs for different MOO problems are ranked based on the best and five good designs, using a number of randomly generated economic scenarios. For details on methodology of parametric uncertainty analysis, interested readers are referred to the literature [24,25,27].

In summary, the main contributions of this study are: integration of SEG, SOFC-GT and cement plant, for the production of electricity and cement (side product), multi-objective optimization of the integrated plant based on four relevant bi-objective problems, selection of final plant design for implementation purpose, using NFM, GRA and parametric uncertainty analysis. The performance of the optimized plant found to be better than reference plant (i.e., gasifier with SOFC-GT).

2. Process simulation of SEG-SOFC-GT plant

In this study, the integrated plant (SEG, SOFC and GT) for producing electricity and heat from Eucalyptus wood chips has been modeled in Aspen Plus simulator. The integrated energy conversion plant has five main parts: (1) sorption enhanced steam biomass gasification coupled with calcium looping for the production of hydrogen-rich gas, (2) hot gas cleaning and steam methane reforming, (3) solid oxide fuel cell with gas turbines to convert hydrogen into electricity, (4) catalytic burning and CO_2 compression, and (5) cement production from purge CaO stream. The main assumptions for simulating SEG-SOFC-GT plant are listed in Table 1.

2.1. The sorption enhanced steam biomass gasification unit

The SEG unit which consists of four reactors: (1) Decomposition, (2) Tar Formation, (3) Gasification, and (4) Regeneration, is shown in Fig. 1. Firstly, biomass feedstock, which is represented as a non-conventional component, is sent to RYIELD (Decomposition) reactor, where it is converted into conventional components, consisting of C, N_2, H_2, O_2, S and ASH, based on the proximate and ultimate analyses. All conventional components produced from biomass are sent to second RYIELD (Tar Formation) reactor to convert carbon, hydrogen and oxygen into tars (i.e., toluene: C_7H_8, naphthalene: $C_{10}H_8$, phenol: C_6H_6O, pyrene: $C_{16}H_{10}$) and unreacted carbon char (C). Then, tars and unreacted carbon char are separated from other residual conventional components. The conventional components without tars and unreacted carbon char are fed into the first RGIBB reactor (Gasification), which simulates gasification using steam (gasifying agent) and CaO for capturing CO_2, as shown in Eqs. (1)–(8). The product stream from biomass gasification is sent to the first cyclone separator for separating solids from the product gases. The product gases from the first cyclone separator are sent to cleaning and reforming unit (unit 2). The solid,

Table 1
Model assumptions for integrated plant.

Section	Specification	Value	Unit	References
Biomass feedstock (Eucalyptus wood)	Proximate analysis (dry weight basis)			[27]
	Volatile matter	78.91	%	
	Fixed carbon	20.72	%	
	ASH	0.37	%	
	Ultimate analysis (dry weight basis)			[27]
	C	57.50	%	
	H	5.30	%	
	O	36.70	%	
	N	0.10	%	
	S	0.03	%	
	ASH	0.37	%	
	Moisture content (weight basis)	8.30	%	[27]
	Higher heating value	19.47	MJ kg^{-1}	[27]
	Lower heating value	18.33	MJ kg^{-1}	[27]
Gasification unit	Pressure drop	0.02	bar	[23]
	Carbon conversion	98	%	[28]
	Gasifier operation pressure	1.50	bar	This paper
	Steam preheat temperature	400	°C	This paper
	Tar production	0.5	g N m^{-3}	[29]
	Tar components (weight basis)			[23]
	Toluene (C_7H_8)	65	%	
	Naphthalene ($C_{10}H_8$)	20	%	
	Phenol (C_6H_6O)	10	%	
	Pyrene ($C_{16}H_{10}$)	5	%	
	Pressure drop cyclone	0.02	bar	[23]
Regeneration unit	Pressure drop	0.02	bar	This paper
	Operating pressure	1.46	bar	This paper
	Operating temperature	900	°C	[29,30]
	Pressure drop cyclone	0.02	bar	[23]
Sulfur removing unit	Pressure drop	0.02	bar	[23]
	Operating pressure	1.46	bar	This paper
	Operating temperature	400	°C	[23,31]
Steam reforming unit	Pressure drop	0.02	bar	[23]
	Operating pressure	1.44	bar	This paper
	Steam preheat temperature	500	°C	This paper
	CH_4 conversion	95	%	[23]
	C_7H_8 conversion	95	%	[23]
	$C_{10}H_8$ conversion	95	%	[23]
	C_6H_6O conversion	95	%	[23]
	$C_{16}O_{10}$ conversion	95	%	[23]
Tar removing unit	Pressure drop	0.02	bar	[23]
SOFC unit	Area	200	cm^2	[32]
	Current density	0.3	A cm^{-2}	[32]
	Operating pressure	1	bar	[22]
	Air excess	2.14	–	[23]
Gas turbine unit	Pressure ratio	5	–	This paper
	Steam excess ratio in the catalytic burner	80	%	[23]
	Isentropic efficiency	85	%	[22]

(continued on next page)

Table 1 (*continued*)

Section	Specification	Value	Unit	References
Cement production unit	Clay composition (weight basis)			[33]
	Silicon dioxide (SiO_2)	61.17	%	
	Alumina oxide (Al_2O_3)	21.64	%	
	Ferric oxide (Fe_2O_3)	9.32	%	
	Calcium oxide (CaO)	1.03	%	
	Magnesium oxide (MgO)	1.68	%	
	Sulfur trioxide (SO_3)	1.15	%	
	Potassium oxide (K_2O)	2.53	%	
	Other (Na_2O + TiO_2)	0.57	%	
	Loss on ignition	0.91	%	[34,35]
	Portland cement composition (weight basis)			
	C_3S	55	%	
	C_2S	18	%	
	C_3A	9	%	
	C_4AF	7	%	
	Gypsum ($CaSO_4$ $2H_2O$)	5	%	
	Others	6	%	
Rotary kiln unit	Operating pressure	1	bar	[35,36]
	Operating temperature	1400	°C	[34–36]
	Preheat temperature	900	°C	This paper

which contains $CaCO_3$, excess CaO, ASH and unreacted carbon char, is sent to second RGIBB (Regenerator) reactor for the regeneration of CaO, as shown in Eq. (9). Oxygen is fed into regenerator for complete combustion of unreacted carbon char, which supplies heat requirement of the calcination reaction. The remaining heat required for calcination reaction is supplied by burner (or post combustor) of SOFC system (unit 3). Finally, the product stream from regenerator is sent to second cyclone separator for separating solids (mainly CaO) from CO_2. Some amount of CaO is purged after regenerator and fresh $CaCO_3$ is added, because CaO will be degraded after several cycles [7,37,38]. In this study, purged CaO stream is fed to a cement production unit (unit 5). Moreover, for recovering mechanical energy, CO_2 stream is fed to a turbine before sending it to CO_2 compression unit (unit 4).

2.2. The hot gas cleaning and steam methane reforming unit

The product stream from SEG unit is fed into gas treatment and steam methane reforming unit as shown in Fig. 2. This unit has three main parts: (1) Hot Gas Cleaning, (2) Steam Reforming, and (3) Tar Removing. The hot gas cleaning unit uses ZnO bed for H_2S removal from product gases (Eq. (10)). Later, product gases with steam are fed into RGIBB (Steam Reforming) reactor, to produce hydrogen from hydrocarbons (Eqs. (11)–(14)) [23]. For recovering mechanical energy, hydrogen-rich gas from steam reforming unit is sent to a scrubber for the removal of tars before sending it to a turbine.

2.3. SOFC-GT unit

The electricity from SOFC-GT system can be produced using hydrogen-rich gas from biomass (via SEG, hot gas cleaning, steam reforming and tar removing) as shown in Fig. 3. This unit has two main parts: (1) a planner SOFC and (2) Cathodic GT (CGT). The hydrogen-rich gas enters on anode side of SOFC, while hot air is fed into cathode side. The hydrogen reacts with oxygen, which is migrated through electrolyte from cathodic side to anodic side, and generates steam and electrons via electrochemical reaction (Eq. (15)). The electrons flow in external circuit from the anodic side to the cathodic side of the fuel cell, and produces direct-current electricity [39]. The SOFC model, which was published by Van herle et al. [40], has water-gas shift (Eq. (4)) and internal steam methane reforming (Eq. (6)) reactions. The electric power output from SOFC can be calculated from available Gibbs free enthalpy flow and irreversible losses, which are ohmic losses, activation and concentration over potentials at anode and cathode (Eqs. (16)–(35)), as shown in Table 2. The excess electricity can be produced

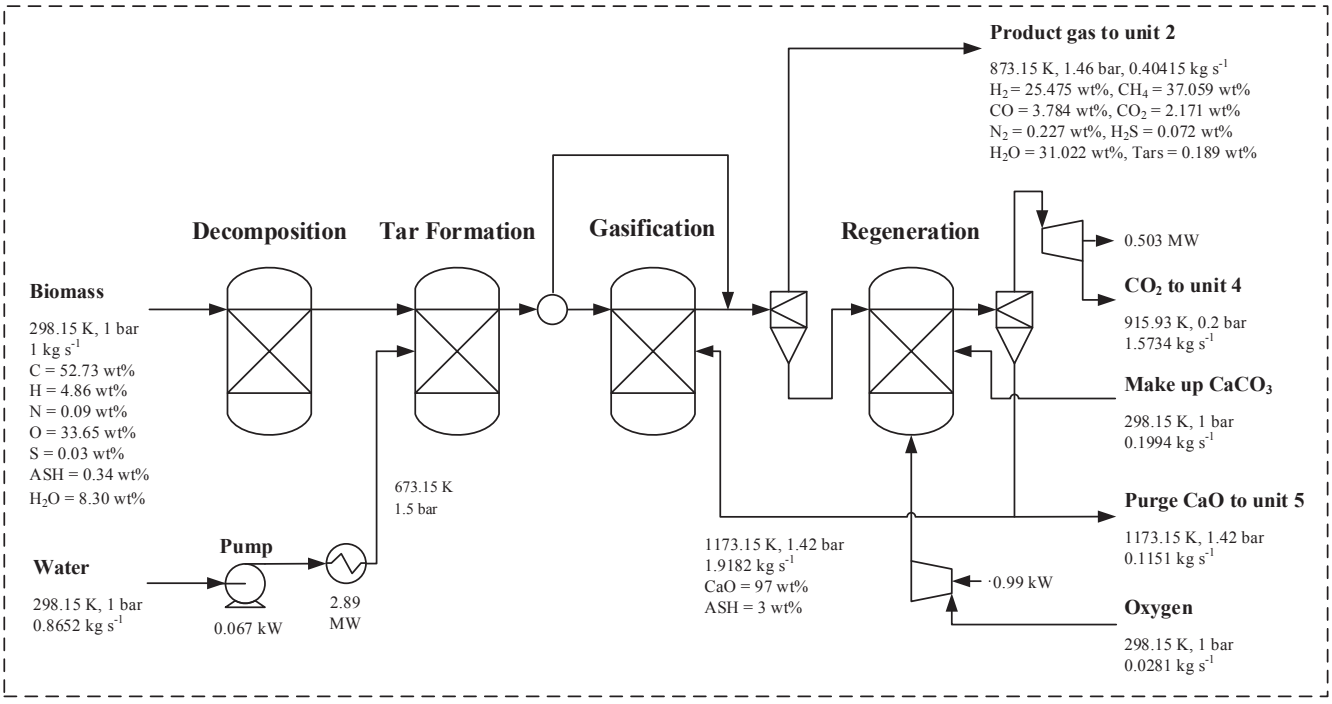

Fig. 1. A simplified schematic of the Sorption Enhanced Steam Biomass Gasification (SEG) (Unit 1).

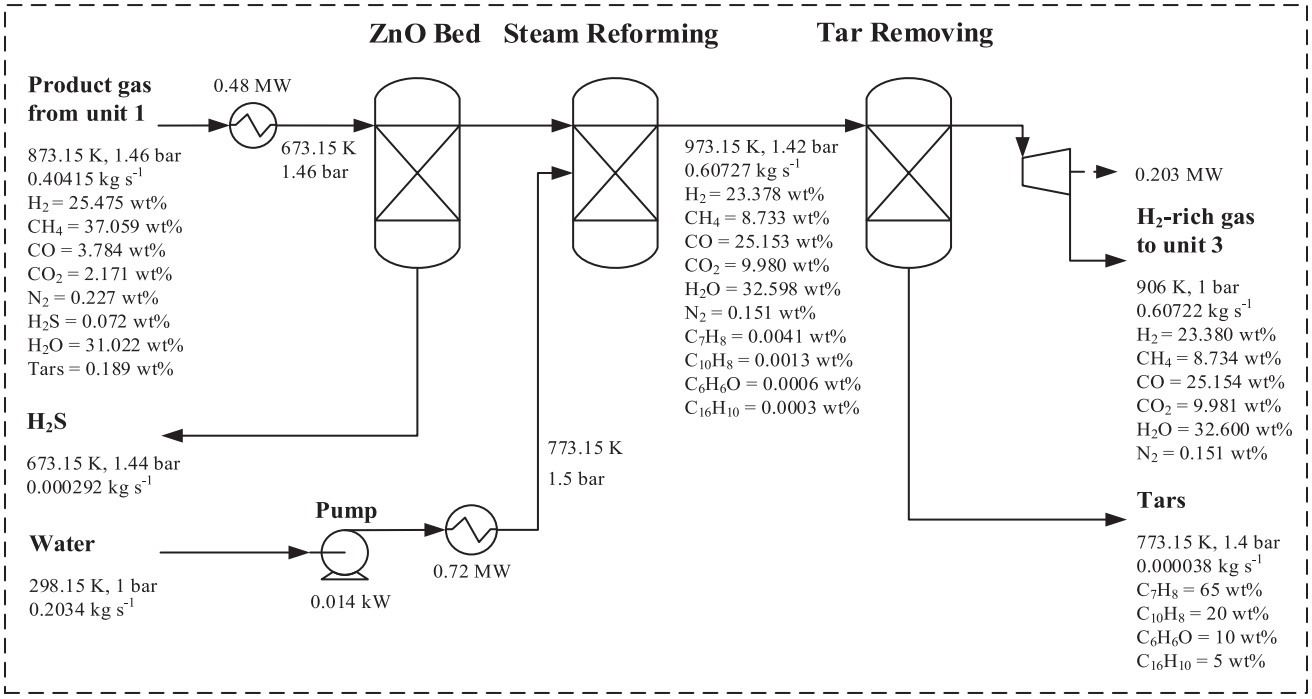

Fig. 2. A simplified schematic of hot gas cleaning and steam reforming (Unit 2).

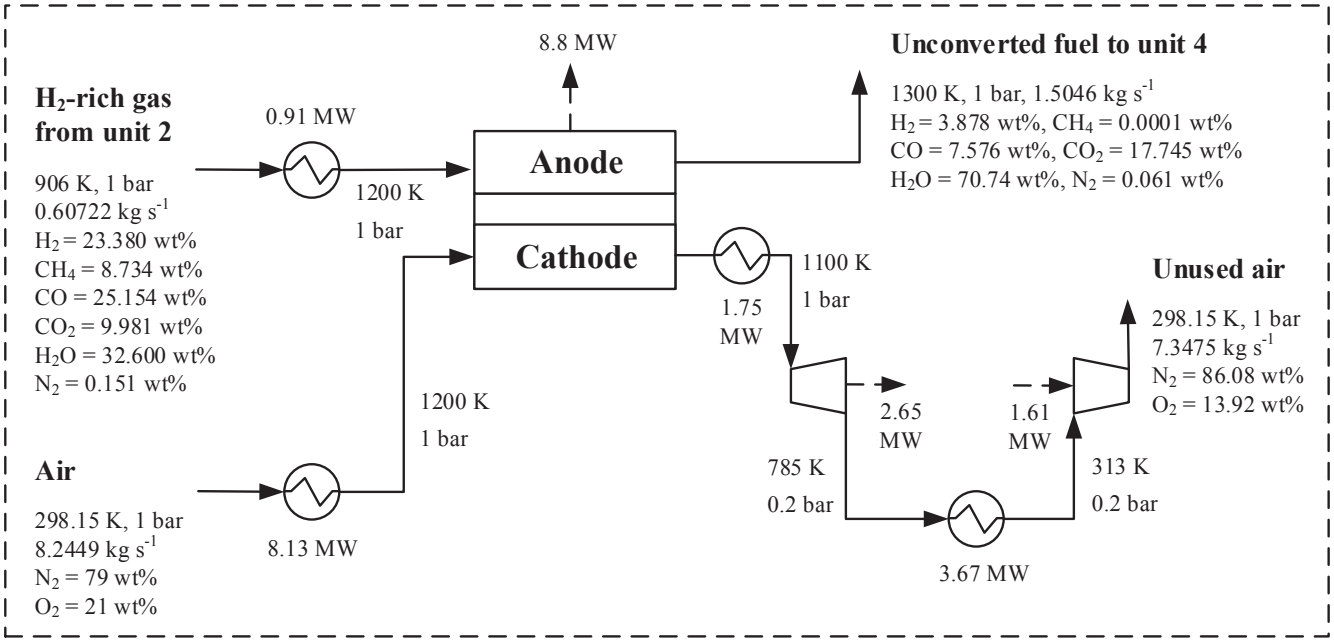

Fig. 3. A simplified schematic of Solid Oxide Fuel Cell (SOFC) – Gas Turbine (GT) (Unit 3).

using unused air from cathodic side of fuel cell by sending air to CGT. Finally, the outlet stream from fuel cell anode is sent to a catalytic burner (unit 4).

Partial oxidation:
$C + 0.5O_2 \leftrightarrow CO$ (1)

Boudouard reaction:
$C + CO_2 \leftrightarrow 2CO$ (2)

Water gas:
$C + H_2O \leftrightarrow CO + H_2$ (3)

Water gas-shift (WGS):
$CO + H_2O \leftrightarrow CO_2 + H_2$ (4)

Methane formation:
$C + 2H_2 \leftrightarrow CH_4$ (5)

Steam methane reforming:
$CH_4 + H_2O \leftrightarrow CO + 3H_2$ (6)

Hydrogen sulfide formation:
$H_2 + S \leftrightarrow H_2S$ (7)

Table 2
Model equations for SOFC [40,49].

	Equations	
Fuel utilization	$U_f = \frac{\dot{n}_{H_2,consumed}}{(\dot{n}_{H_2,a,in} + \dot{n}_{CO,a,in} + 4\dot{n}_{CH_4,a,in})}$	(16)
	$\dot{n}_{H_2,consumed} = (\dot{n}_{H_2,a,in} + \dot{n}_{CO,a,in} + 4\dot{n}_{CH_4,a,in}) - (\dot{n}_{H_2,a,out} + \dot{n}_{CO,a,out} + 4\dot{n}_{CH_4,a,out})$	(17)
	or	(18)
	$\dot{n}_{H_2,consumed} = 2(\dot{n}_{O_2,c,in} - \dot{n}_{O_2,c,out})$	
Current	$I = JA_{cell}$	(19)
	where J is 0.3 A cm^{-2} and A_{cell} is 200 cm^2.	
Number of cells	$N_{cells} = \frac{4\dot{n}_{H_2,consumed}}{I}$	(20)
Power	$\dot{W}_{SOFC} = -\Delta\dot{G}_{stack} - \eta_{ohm} - (\eta_{act,a} + \eta_{act,c} + \eta_{diff,a} + \eta_{diff,c})N_{cells}I$	(21)
Available Gibbs free energy	$\Delta\dot{G}_{stack} = (\dot{G}_{c,out} + \dot{G}_{a,out}) - (\dot{G}_{c,in} + \dot{G}_{a,in})$	(22)
Ohmic losses	$\eta_{ohm} = R_{tot}^2 I^2$	(23)
	$R_{tot} = R_I + R_E$	(24)
	$R_I = \frac{R_{I,a} + R_{I,c}}{A_{cell}} N_{cells}$	(25)
	$R_E = \frac{L_E}{\sigma_E A_{cell}} N_{cells} f_{CC}$	(26)
	$\sigma_E = \sigma_{0,E} \exp\left(-\frac{E_{A,E}}{RT}\right)$	(27)
	where $R_{I,a}$ is 0.02 Ω cm^2, $R_{I,c}$ is 0.03 Ω cm^2, L_E is 0.001, f_{CC} is 4, $\sigma_{0,E}$ is 372.33 S cm^{-1} and $E_{A,c}$ is 79535 J mol^{-1}.	
Cathode activation loss	$\eta_{act,c} = \frac{RT}{F} \sinh^1\left(\frac{J}{J_{0,c}}\right)$	(28)
	$J_{0,c} = \frac{2RT\sigma_c}{F}$	(29)
	$\sigma_c = \sigma_{0,c} \exp\left(-\frac{E_{A,c}}{R}\left(\frac{1}{T} - \frac{1}{923.15}\right)\right)$	(30)
	where $\sigma_{0,c}$ is 8.602 S cm^{-1} and $E_{A,c}$ is 101205 J mol^{-1}.	
Anode activation loss	$\eta_{act,a} = \frac{RT}{F} \sinh^1\left(\frac{J}{J_{0,a}}\right)$	(31)
	$J_{0,a} = \frac{RT\sigma_a}{3F}$	(32)
	$\sigma_a = \sigma_{0,a} \exp\left(-\frac{E_{A,a}}{RT}\right)$	(33)
	where $\sigma_{0,a}$ is 433030 S cm^{-1} and $E_{A,a}$ is 106000 J mol^{-1}.	
Cathode polarization loss	$\eta_{diff,c} = \frac{-RT}{2F} \log(1 - U_f)$	(34)
Anode polarization loss	$\eta_{diff,a} = \frac{-RT}{2F} \log\left(1 - \frac{U_f}{\lambda}\right)$	(35)
	where λ is 2.14.	

Carbonation:
$CaO + CO_2 \leftrightarrow CaCO_3$ (8)

Calcination:
$CaCO_3 \leftrightarrow CaO + CO_2$ (9)

Desulfurizing:
$H_2S + ZnO \rightarrow H_2O + ZnS$ (10)

Toluene hydrolysis:
$2C_7H_8 + 21H_2O \leftrightarrow 7CO + 7CO_2 + 29H_2$ (11)

Naphthalene hydrolysis:
$C_{10}H_8 + 15H_2O \leftrightarrow 5CO + 5CO_2 + 19H_2$ (12)

Phenol hydrolysis:
$C_6H_6O + 8H_2O \leftrightarrow 3CO + 3CO_2 + 11H_2$ (13)

Pyrene hydrolysis:
$C_{16}H_8 + 24H_2O \leftrightarrow 8CO + 8CO_2 + 29H_2$ (14)

Electrochemical:
$H_2 + 0.5O_2 \rightarrow H_2O$ (15)

2.4. Catalytic burning and CO_2 compression unit

The outlet stream from fuel cell anode, which has unconverted fuel, enters into catalytic burning and CO_2 compression unit as shown in Fig. 4. The unconverted fuel is reacted with oxygen in a catalytic burner, and generated heat is used as a hot utility in the integrated energy plant. The exhaust stream from burner is sent to Anodic GT (AGT) for producing electricity. Finally, the outlet stream of AGT is sent to remove water before combining with CO_2 stream from Regeneration (SEG unit), and combined stream is sent to compression unit to be stored as a compressed CO_2 product. The product CO_2 can be used to grow biomass and convert renewable electricity or H_2 into green fuels for storage purpose [23].

2.5. Cement production unit

The purge CaO stream from regenerator (SEG unit) is sent to cement production unit. The cement production unit has three main parts: (1) Raw Mill, (2) Rotary Kiln and (3) Cement Mill, as shown in Fig. 5. The clay, which contains silicon dioxide (SiO_2), alumina oxide (Al_2O_3), ferric oxide (Fe_2O_3) and other materials is crushed and milled into a raw mill. The product of raw mill is blended and heated in a preheater, and then mixed with purged CaO from SEG unit. The mixture is sent to a rotary kiln, also called as clinker burning. The chemical reactions, which occur in rotary kiln, are illustrated in Eqs. (36)–(39). Heat is required to melt and to form final product (called as clinker), and it comes from catalytic burner. The final product from rotary kiln is cooled down and sent to a cement mill together with gypsum. The Portland cement is stored in silos before it is delivered for construction.

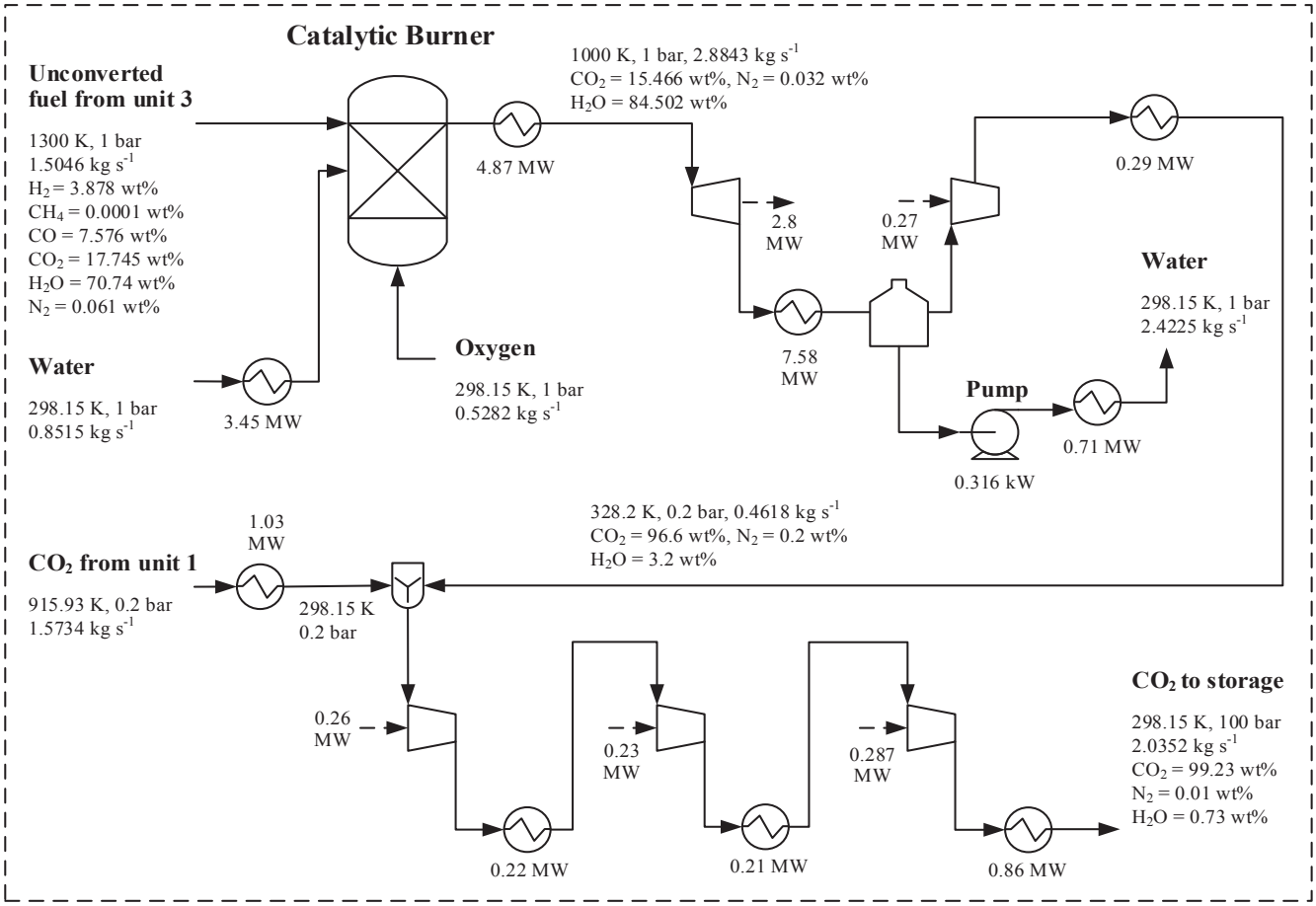

Fig. 4. A simplified schematic of catalytic burning and CO_2 compression (Unit 4).

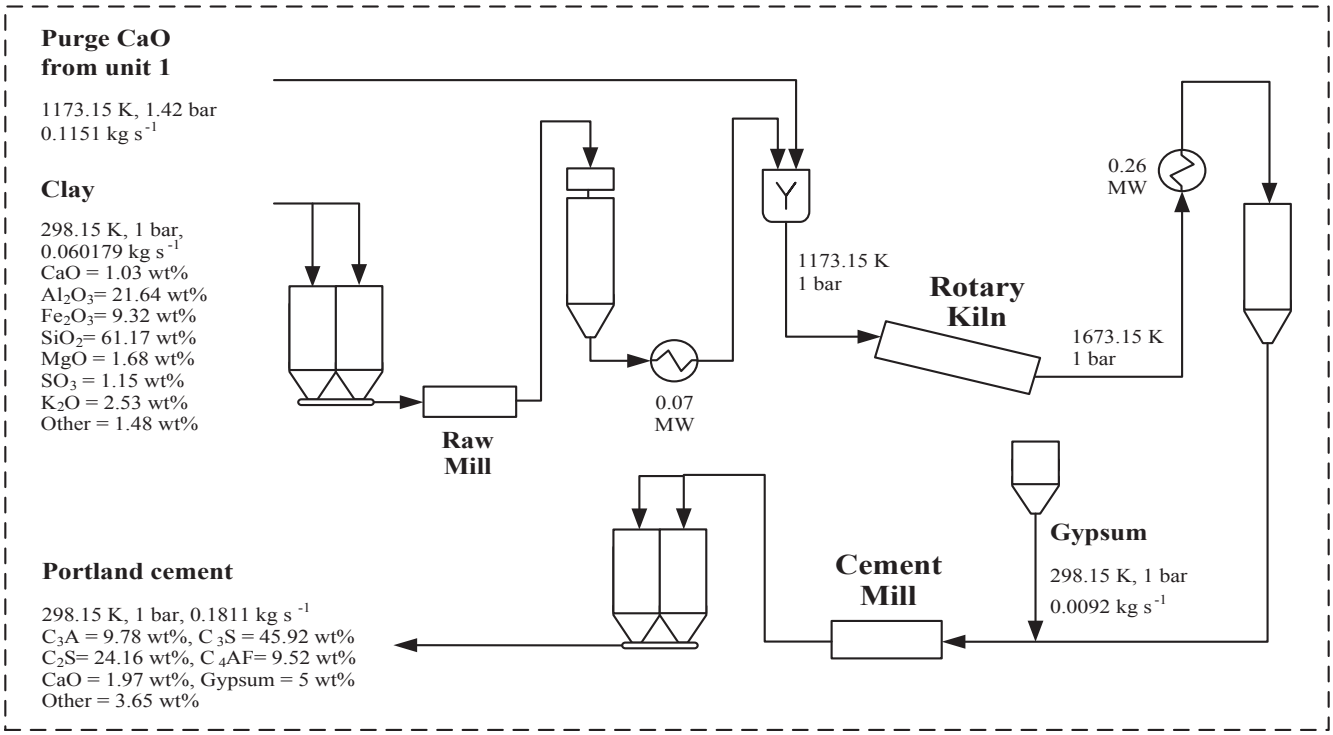

Fig. 5. A simplified schematic of cement production (Unit 5).

C_2S formation:

$$2CaO + SiO_2 \rightarrow C_2S \quad (36)$$

C_3S formation:

$$CaO + C_2S \rightarrow C_3S \quad (37)$$

C_3A formation:

$$3CaO + Al_2O_3 \rightarrow C_3A \quad (38)$$

C_4AF formation:

$$4CaO + Al_2O_3 + Fe_2O_3 \rightarrow C_4AF \quad (39)$$

3. Exergy analysis

The energy analysis method is based on the first law of thermodynamics while the exergy analysis method is based on the first and second laws of thermodynamics. Energy is a measure of only the quantity whereas exergy also takes into account the quality of energy. Moreover, exergy analysis can be used to identify and quantify the locations, causes and magnitudes of inefficiencies in process. Therefore, the exergy analysis method is used to enhance system understanding and to examine the possibility of process optimization. In the present study, the integrated energy conversion plant is assumed to be at steady state and isothermal conditions. The energy balance can be written by Eqs. (40)–(42).

$$\sum_{in} \dot{E}n = \sum_{out} \dot{E}n \quad (40)$$

$$\sum_{in} \dot{E}n = \dot{E}n_{biomass} + \dot{E}n_{water,gas} + \dot{E}n_{water,ref} + \dot{E}n_{make-up} + \dot{E}n_{O_2,reg} + \dot{E}n_{air,c} + \dot{E}n_{water,com} + \dot{E}n_{O_2,com} + \dot{E}n_{clay} + \dot{E}n_{gypsum} + \dot{Q}_{in} \quad (41)$$

$$\sum_{out} \dot{E}n = \dot{E}n_{water,out} + \dot{E}n_{unusedair} + \dot{E}n_{H_2S} + \dot{E}n_{tars} + \dot{E}n_{cement} + \dot{E}n_{CO_2} + \dot{Q}_{out} + \dot{W} \quad (42)$$

By neglecting change in the kinetic and potential energies, three categories of exergy transfer are considered: exergy transfer with heat transfer ($\dot{E}x_{\dot{Q}}$), exergy transfer with work or electricity production ($\dot{E}x_{\dot{W}}$,$\dot{W}$), and exergy transfer with material flow ($\dot{E}x$). The exergy transfer for heat transfer can be calculated by Eq. (43) [41].

$$\dot{E}x_{\dot{Q}} = \dot{Q}\left(1 - \frac{T_0}{T}\right) \quad (43)$$

where $\dot{Q}$ is heat transferred into system (kJ h^{-1}); T_0 is reference temperature (298.15 K); T is operating temperature (K). The exergy transfer for work done can be calculated by Eq. (44) [41].

$$\dot{E}x_{\dot{W}} = \dot{W} \quad (44)$$

where $\dot{W}$ is mechanical work rate (kJ h^{-1}). The exergy transfer for material flow of stream i ($\dot{E}x_i$) can be calculated by Eq. (45).

$$\dot{E}x_i = \dot{n}_i ex_i \quad (45)$$

where $\dot{n}_i$ and ex_i are molar flow rate (kmol h^{-1}) and specific exergy transfer for material flow of stream i (kJ $kmol^{-1}$). The specific exergy transfer for the mass flow of stream i is sum of the specific physical (ex_{ph}) and specific chemical (ex_{ch}) exergies, as shown in Eq. (46) [42,43].

$$ex_i = ex_{ph,i} + ex_{ch,i} \quad (46)$$

The specific physical exergy is the amount of useful work obtainable by passing one mole of a material from its initial state (T,P) to environment state (T_0, P_0) and can be calculated by Eq. (47).

$$ex_{ph,i} = (h - h_0) - T_0(s - s_0) \quad (47)$$

where h is specific enthalpy (kJ $kmol^{-1}$) and s is specific entropy (kJ $kmol^{-1}$ K^{-1}) at initial state (T,P). Moreover, h_0 is specific enthalpy (kJ $kmol^{-1}$) and s_0 is specific entropy (kJ $kmol^{-1}$ K^{-1}) at environment state (298.15 K, 1 atm).

The specific chemical exergy is the amount of work generated when all material in the system is reacted at the environment state (T_0, P_0), and can be calculated by Eq. (48) [42,43].

$$ex_{ch,i} = \sum y_j ex_{ch,j} + RT_0 \sum y_j \ln(y_j) \quad (48)$$

where y_j is mole fraction and $ex_{ch,j}$ is specific chemical exergy of j^{th} component in stream i. The exergy transfer for mass flow of biomass ($\dot{E}x_{biomass}$) can be calculated by Eq. (49).

$$\dot{E}x_{biomass} = \beta \dot{M}_{biomass} LHV_{biomass} \quad (49)$$

where β is ratio of biomass chemical exergy and LHV. Based on the literature [42,44–45], β is calculated using correlation of mass fractions of carbon, hydrogen, nitrogen and oxygen in biomass, as shown in Eq. (50).

$$\beta = \frac{1.044 + 0.016\left(\frac{H}{C}\right) - 0.3493\left(\frac{O}{C}\right)\left(1 + 0.0531\left(\frac{H}{C}\right)\right) + 0.0493\left(\frac{N}{C}\right)}{1 - 0.4124\left(\frac{O}{C}\right)} \quad (50)$$

The exergy balance can be written by Eqs. (51)–(55) [42].

$$\sum_{in} \dot{E}x = \sum_{out} \dot{E}x + \sum_{des} \dot{E}x \quad (51)$$

$$\sum_{in} \dot{E}x = \dot{E}x_{biomass} + \sum_{in} \dot{n}_i ex_i + \dot{E}x_{\dot{Q}} \quad (52)$$

$$\sum_{in} \dot{n}_i ex_i = \dot{n}_{water,gas} ex_{water,gas} + \dot{n}_{water,ref} ex_{water,ref} + \dot{n}_{make-up} ex_{make-up} + \dot{n}_{O_2,reg} ex_{O_2,reg} + \dot{n}_{air,c} ex_{air,c} + \dot{n}_{water,com} ex_{water,com} + \dot{n}_{O_2,com} ex_{O_2,com} + \dot{n}_{clay} ex_{clay} + \dot{n}_{gypsum} ex_{gypsum} \quad (53)$$

$$\sum_{out} \dot{E}x = \dot{E}x_{\dot{W}} + \sum_{out} \dot{n}_i ex_i \quad (54)$$

$$\sum_{out} \dot{n}_i ex_i = \dot{n}_{water,out} ex_{water,out} + \dot{n}_{unusedair} ex_{unusedair} + \dot{n}_{H_2S} ex_{H_2S} + \dot{n}_{tars} ex_{tars} + \dot{n}_{cement} ex_{cement} + \dot{n}_{CO_2} ex_{CO_2} \quad (55)$$

where $\sum_{des} \dot{E}x$ is total exergy destruction rate (kJ h^{-1}).

In this study, exergy efficiency of electricity production (η_{EX}) is used as an objective function that can be calculated by Eq. (56) [46].

$$\eta_{EX} = \left(\frac{\dot{E}x_{\dot{W}}}{\sum_{in} \dot{E}x}\right) \times 100\% \quad (56)$$

4. Optimization problem formulation

The formulated MOO problems for SEG-SOFC-GT plant is shown in Table 3 (Eqs. (57)–(62)). In this study, four important bi-objective optimization problems are studied: (1) maximization of annual profit, minimization of ACC, (2) maximization of exergy efficiency, minimization of ACC, (3) minimization of both ACC and operating cost, and (4) minimization of both levelized electricity cost and ACC per kWh. Here, the method of economic analysis is annual profit, which has been defined based on the estimated receipts (income) and disbursements (costs) during the life cycle of the plant. All the units of the integrated energy plant are shown in Figs. 1–5. Each MOO problem has nine decision variables, and values of decision variables bounds are chosen by preliminary analysis and literature reviews [7,23,28–31,37,38].

The MOO of the integrated SEG-SOFC-GT plant has been studied by the use of OSMOSE platform (Fig. 6). OSMOSE has four parts. The first part is MOO program based on genetic algorithms with clustering [47,48]. The second part is process simulation in Aspen Plus for the modeling of integrated SEG-SOFC-GT plant. The third part is heat integration, to calculate minimum energy requirements, minimum

Table 3
MOO problem formation for SEG-SOFC-GT plant.

Objective functions		
MOO P1:	Maximize Annual Profit ($ year^{-1}) Minimize Annualized Capital Cost ($ year^{-1})	
MOO P2:	Maximize Exergy Efficiency (%) Minimize Annualized Capital Cost ($ year^{-1})	
MOO P3:	Minimize Annualized Capital Cost ($ year^{-1}) Minimize Operating Cost ($ year^{-1})	
MOO P4:	Minimize Levelized Electricity Cost (LEC) ($ kWh^{-1}) Minimum Annualized Capital Cost per kWh ($ year^{-1} kWh^{-1})	
where		
Annual profit = Product sale – ACC – Annual Operating Cost (AOC)		(57)
Product sale = Electricity production ($ year^{-1}) + Portland cement ($ year^{-1})		(58)
AOC = Raw Materials + Utilities		(59)
Raw materials = Biomass (Wood) + O_2 + $CaCO_3$ (Make-up) + Clay + Gypsum		(60)
LEC = (ACC + AOC)/Electricity production (kWh)		(61)
ACC per kWh = ACC/Electricity production (kWh)		(62)

Decision variables	**Lower bound**	**Upper bound**
Steam to carbon ratio for gasifier (–)	0.95	1.20
Gasifier temperature (K)	873.15	973.15
CaO to carbon ratio for gasifier (–)	0.65	1.00
Steam to carbon ratio for reformer (–)	1.80	2.40
Reformer temperature (K)	973.15	1023.15
SOFC temperature (K)	1050	1200
Fuel utilization (–)	0.60	0.75
Anodic GT inlet temperature (K)	1000	1300
Cathodic GT inlet temperature (K)	800	1100

number of units and heat exchange area by using data of flow rates and temperatures of selected streams from the SEG-SOFC-GT plant simulation. The last part is performance evaluation, to calculate objectives by using decision variables, heat integration results, data from plant simulation, operating limits and market considerations.

The correlations and data found in Rodriguez et al. [36], Maréchal et al. [49], Pelster [50], Ulrich and Vasudevan [51], Turton et al [52], Cormos [53] and Alyasri et al. [54] are used to calculate ACC of the integrated SEG-SOFC-GT plant. In the MOO study of the proposed energy plant, below given values of the plant operating conditions and market economics are used [22,23,24,26]: interest rate, IR = 0.06 (%); yearly operating time of plant, YO = 6600 (h y^{-1}); SOFC and gasifier life time, LT1 = 6 (y); life time of other equipment, LT2 = 18 (y); oxygen price, OXYP = 0.065 ($ kg^{-1}); $CaCO_3$ price, CACO3P = 0.0245 ($ kg^{-1}); wood price, WP = 0.1 ($ kg^{-1}); electricity price, ELP = 0.16 ($ kWh^{-1}); Portland cement price, CMP = 0.075 ($ kg^{-1}). The integrated plant has 12 MW of electricity production, and the feed or biomass consumption rate for this plant is 1 kg s^{-1}.

5. Optimization results

5.1. Maximization of annual profit, minimization of ACC

The optimization results for the simultaneous maximization of annual profit and minimization of ACC (MOO problem 1) are presented in Fig. 7. These results were found using OSMOSE: population size, NP = 50; number of function evaluations, NFE = 3000. As anticipated, both these objective functions (annual profit, ACC) are conflicting with each other. This figure also presents changes in the main decision variables with annual profit. Temperature of gasifier, fuel utilization in SOFC, and inlet temperatures of anodic and cathodic turbines (AGT, CGT) are mainly responsible for the shape of the Pareto front. S/C (steam to carbon) ratio for gasifier and temperature of SOFC are near to their upper bounds, whereas S/C ratio for reformer and reformer temperature are near to their lower bounds. Hence, these four variables are not presented in Fig. 7 for conciseness. CaO/C ratio for gasifier is also constant at the optimal value. The hydrogen production from SEG increases with increase in the gasifier temperature due to the prominent effects of water gas-shift and methane formation reactions (Eqs. (4) and (5)), which gives more hydrogen production and power generation. Moreover, with increase in the fuel utilization, power generation from SOFC increases due to larger consumption of hydrogen in the electrochemical reaction (Eq. (14)). This increase in the power generation lead to increase in the yearly profit and the ACC.

5.2. Maximization of exergy efficiency, minimization of ACC

For MOO problem 2, Pareto-optimal solutions obtained for simultaneous optimization of exergy efficiency (maximization) and ACC (minimization) are shown in Fig. 8. These results were found using OSMOSE: population size, NP = 50; number of function evaluations, NFE = 3000. It can be seen that exergy efficiency is conflicting with the ACC. The proposed plant shows very good exergy efficiency, with maximum value 61.2%. Fig. 8 also shows changes in five decision variables with exergy efficiency. Gasifier temperature, CaO/C ratio for gasifier, fuel utilization in SOFC, and inlet temperatures of anodic and cathodic turbines (AGT, CGT) are main contributors in the shape of the Pareto front. S/C ratio for reformer and reformer temperature are near to their lower bounds, whereas S/C ratio for gasifier and temperature of SOFC are near to their upper bounds. Hence, these four variables are not presented for conciseness. The exergy efficiency and annualized capital cost increase with increase in the gasifier temperature and fuel utilization. This is because, higher gasifier temperature has positive effect on the hydrogen production and the power generation. In addition, the higher fuel utilization has a significant positive impact on the power generation.

5.3. Minimization of both ACC and operating cost

Fig. 9 shows the optimization results for the simultaneous minimization of both ACC and operating cost (MOO problem 3). These results were found using OSMOSE: population size, NP = 50; number of

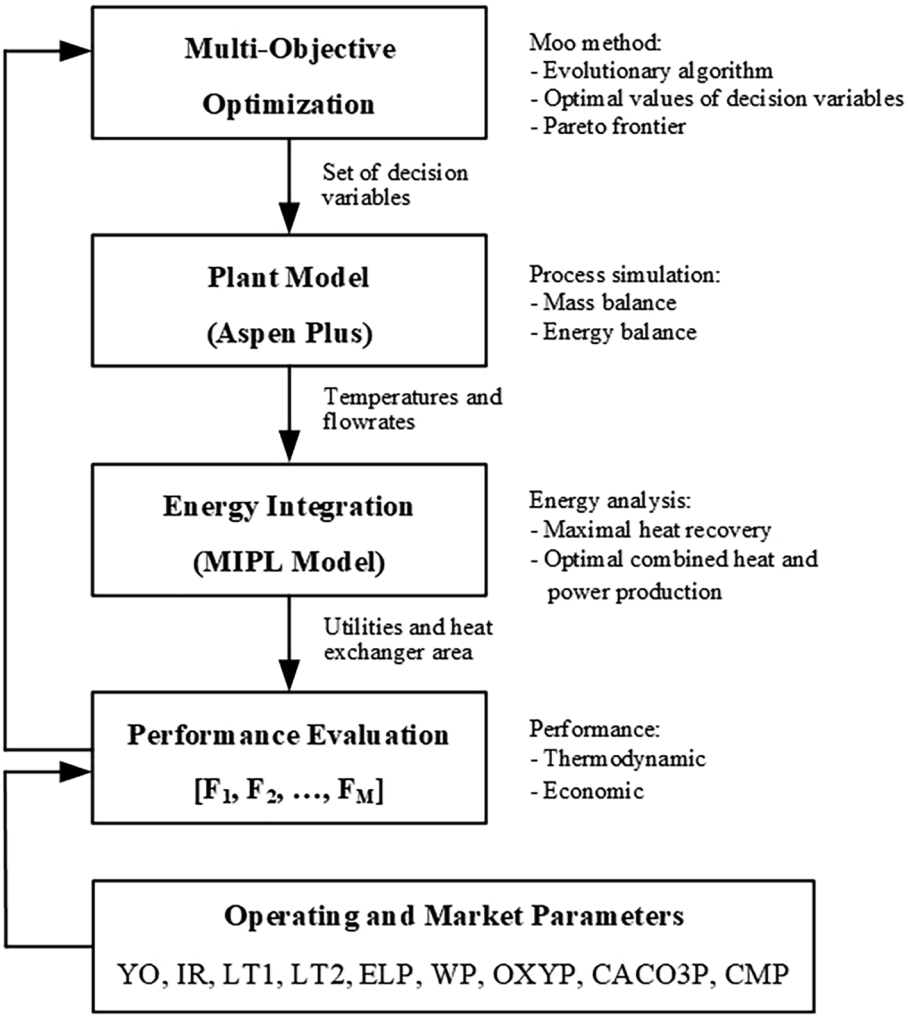

Fig. 6. OSMOSE platform: MOO approach used for the integrated SEG-SOFC-GT plant.

function evaluations, NFE = 3000. It can be noticed that ACC and operating cost are conflicting with each other. Fig. 9 also shows changes in five decision variables with the ACC. Gasifier temperature, CaO/C ratio for gasifier, fuel utilization in SOFC, and inlet temperatures of anodic and cathodic turbines (AGT, CGT) are main contributors in the shape of the Pareto front. S/C ratio for gasifier and temperature of SOFC are near to their upper bounds, whereas S/C ratio for reformer and reformer temperature are near to their lower bounds. Hence, these four variables are not presented in Fig. 9 for conciseness. In Fig. 9, the Pareto front can be divided into two parts. In the first part (left hand side), increase in the annualized capital cost and sharp decrease in the operating cost, is due to increase in the fuel utilization. The fuel utilization has a positive effect on the power generation, and it increases the capital cost of fuel cell and reduces cost of oxygen for the catalytic burning unit. In the second part of the Pareto front (right hand side), a sharp increase in the annualized cost and decrease in the operating cost, is due to the CaO/C ratio for the gasifier. The lower value of the CaO/C ratio reduces the cost of fresh $CaCO_3$, but it increases the capital cost of the gas cleaning and steam methane reforming units.

5.4. Minimization of both levelized electricity cost and ACC per kWh

For studying the effect of plant capacity on the electricity price, MOO of the proposed SEG-SOFC-GT plant (or MOO problem 4) is studied for simultaneous minimization of both levelized electricity cost and ACC per kWh. For three typical plant capacities, ranges of both objective functions obtained via MOO, are presented in Table 4. As anticipated, the electricity production price for large size plant will be lower. The levelized electricity cost and ACC per kWh of the proposed energy plant are lower compared to the reference plant, i.e., integrated gasifier and SOFC-GT plant [23] with the same plant capacities. The reasons for this difference are: feedstocks, the ranges of decision variables and technology used in the biomass gasification part. In this study, biomass feedstock has lower moisture content compared to the reference case, and SEG technology coupled with calcium looping for production of hydrogen-rich gas can reduce the tar content in the product gas. This reduces the feedstock cost, and also the capital cost of hot gas cleaning and steam reforming units.

6. Ranking of Pareto solutions of the integrated SEG-SOFC-GT plant

The solution of a MOO problem is a set of Pareto solutions, collectively called as Pareto front. All the Pareto solutions are equally good mathematically, and each solution represents a distinct plant design. In order to implement these results in practice, decision makers have to select one of the Pareto solutions. The selection of Pareto solution may be performed based on the judgement of decision makers, or using a ranking method that usually provides few solutions, based on the provided knowledge. In this work, two methods namely, net flow method and gray relational analysis are used for the ranking of the Pareto solutions.

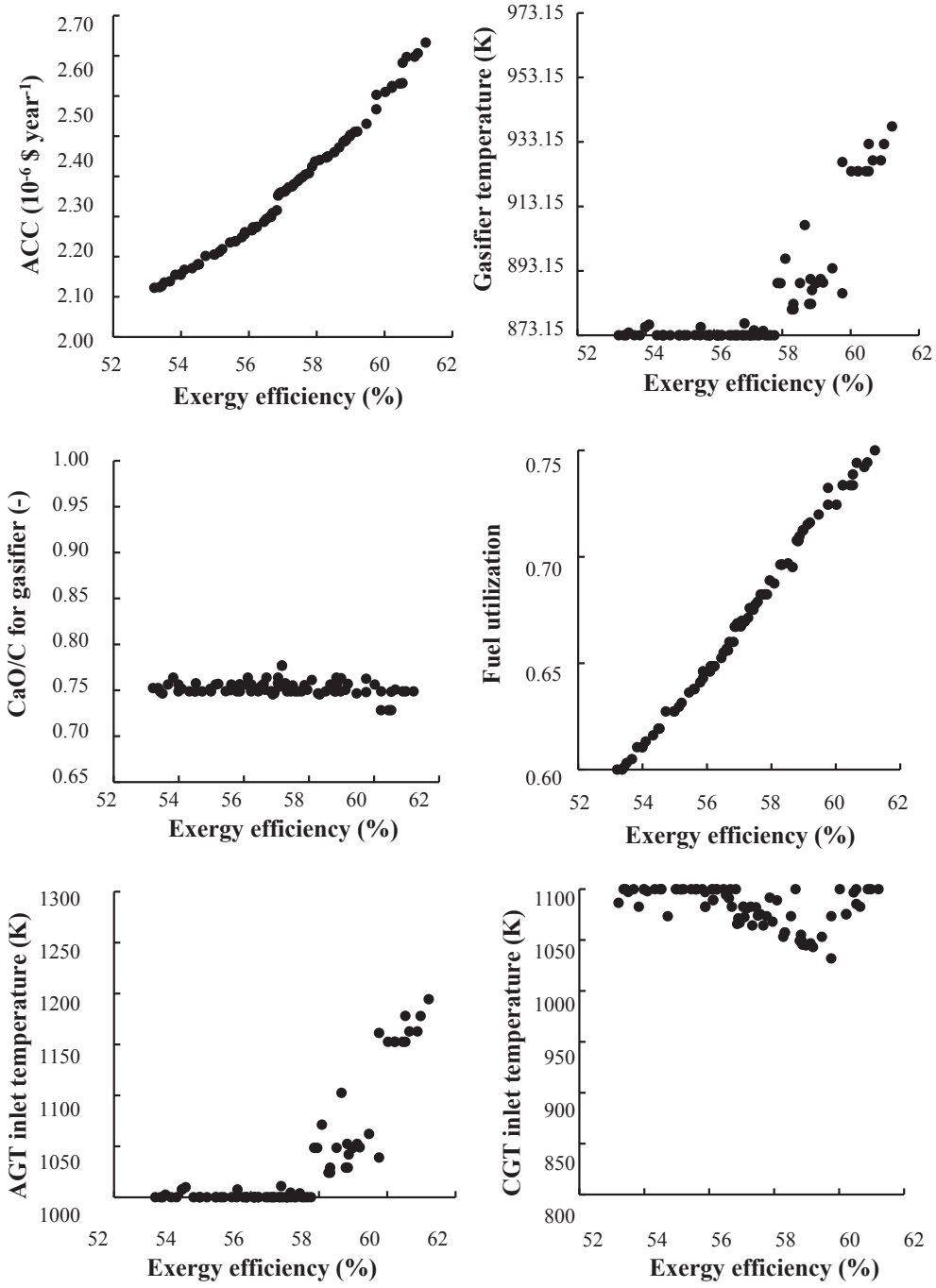

Fig. 7. Optimization results for the integrated SEG-SOFC-GT plant for MOO problem 1.

6.1. Net flow method (NFM) and gray relational analysis (GRA)

In net flow method, experience of the decision maker is employed in defining four ranking parameters for each objective: weights, W_j; indifference threshold, Q_j; preference threshold, P_j; veto threshold: V_j. The values of the indifference, preference and veto thresholds are set (by the decision maker) as 10.0%, 20.0% and 80.0% of the optimal objective function ranges, respectively [25,55,56]. Firstly, the concordance and discordance indices are determined for each pair of solutions using four ranking parameters (weight, indifference threshold, preference threshold and veto threshold). After that, relative performance is calculated for each pair of solutions using the concordance and discordance indices. Finally, for each Pareto solution, ranking score is calculated using relative performance of solution. The Pareto solution, having best ranking score, is the recommended solution. On the other hand, GRA is used to combine all the considered performance characteristics into a single value that can be used as a single characteristic in the decision-making. GRA is typically applied in three steps: normalization of the objective values of the Pareto front, defining the ideal sequence and evaluating grey rational coefficient (GRC) values for all solutions. The optimal solution, having largest GRC value, is the recommended solution [25]. Contrary to NFM, GRA does not require any input (e.g., weights and threshold values) from the decision maker. Table 5 presents values of NFM input parameters to rank the optimal solutions of the integrated energy plant, for each MOO problem.

Fig. 10(a) shows the recommended optimal Pareto solutions for MOO problem 1, using NFM and GRA methods. In case of higher weight for annual profit (W_1 = 0.75), NFM recommends Pareto solution with

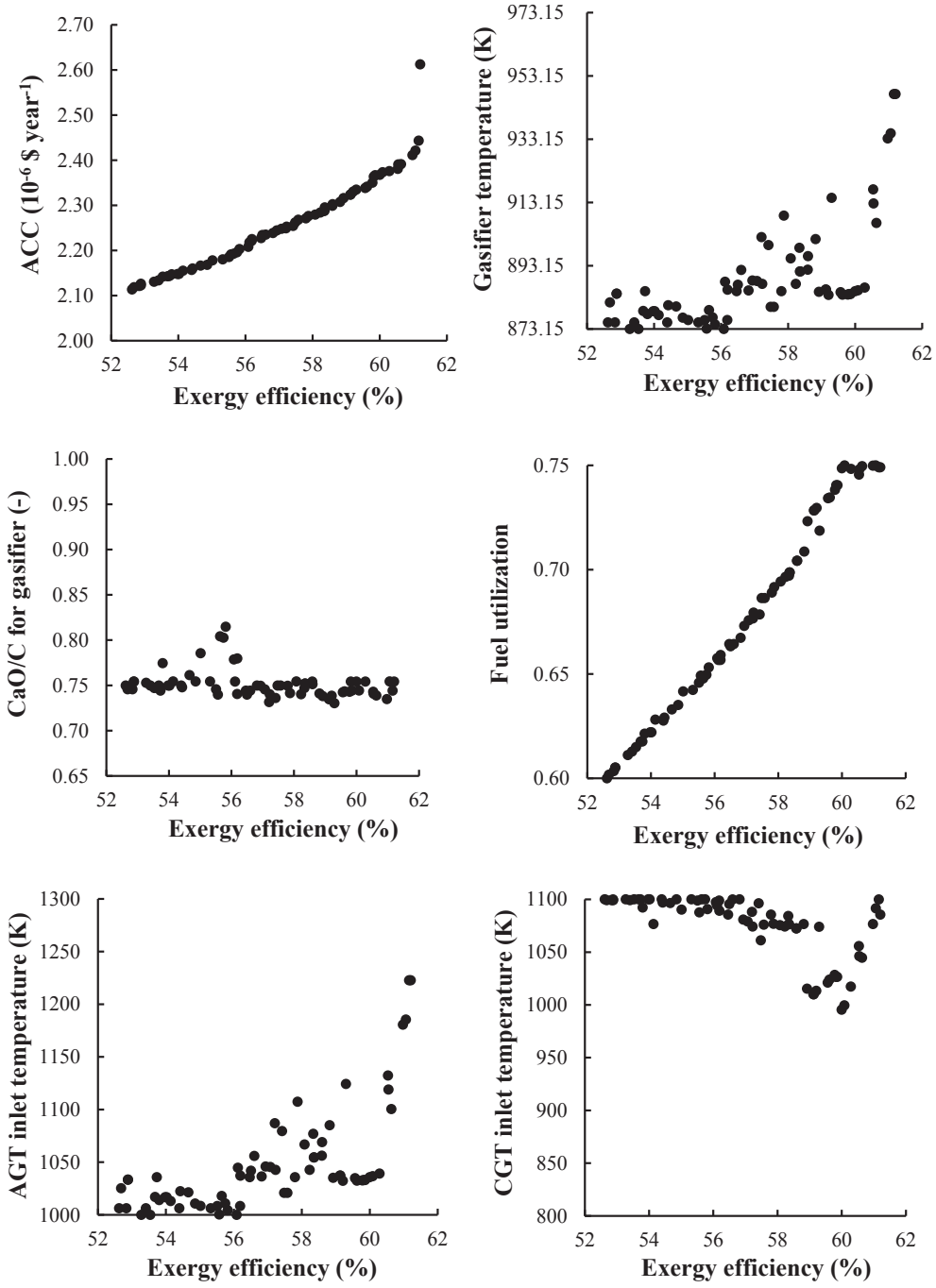

Fig. 8. Optimization results for the integrated SEG-SOFC-GT plant for MOO problem 2.

higher annual profit value. Conversely, NFM recommends Pareto solution with lower annual profit for lower annual profit weight (W_1 = 0.25). Moreover, GRA method recommends Pareto solution with lowest annual profit value compared to three recommended Pareto solutions (using three different weights) by NFM. For MOO problem 2, the preferred Pareto solutions obtained via NFM and GRA methods are shown in Fig. 10(b). With exergy efficiency having a weightage of 0.25, NFM suggests Pareto solution with lower exergy efficiency value. As anticipated, NFM suggests Pareto solutions with higher exergy efficiencies for high weightage of exergy efficiency (W_1 = 0.50 and 0.75). Nevertheless, GRA method recommend a Pareto solution which is close to the recommended Pareto solution by NFW with exergy efficiency weight = 0.75.

Fig. 10(c) presents the recommended Pareto solutions for MOO problem 3, using NFM and GRA methods. In case of higher weight for annualized capital cost (W_1 = 0.75), NFM recommends Pareto solution with lower value of annualized capital cost. Interestingly, NFM recommends same Pareto solution using lower weight for annualized capital cost (W_1 = 0.25) and equal weights for both objectives (W_1 = 0.50). Moreover, in Fig. 10(c), it can also be noticed that the recommended Pareto solution by GRA method is quite close to the recommended Pareto solution by NFM using W_1 = 0.25, 0.50. Fig. 10(d) presents the recommended Pareto solutions for MOO problem 4, using NFM and GRA methods. With higher weight for levelized electricity cost (W_1 = 0.75), NFM suggests Pareto solution with lower value of levelized electricity cost. As anticipated, using lower weight for levelized

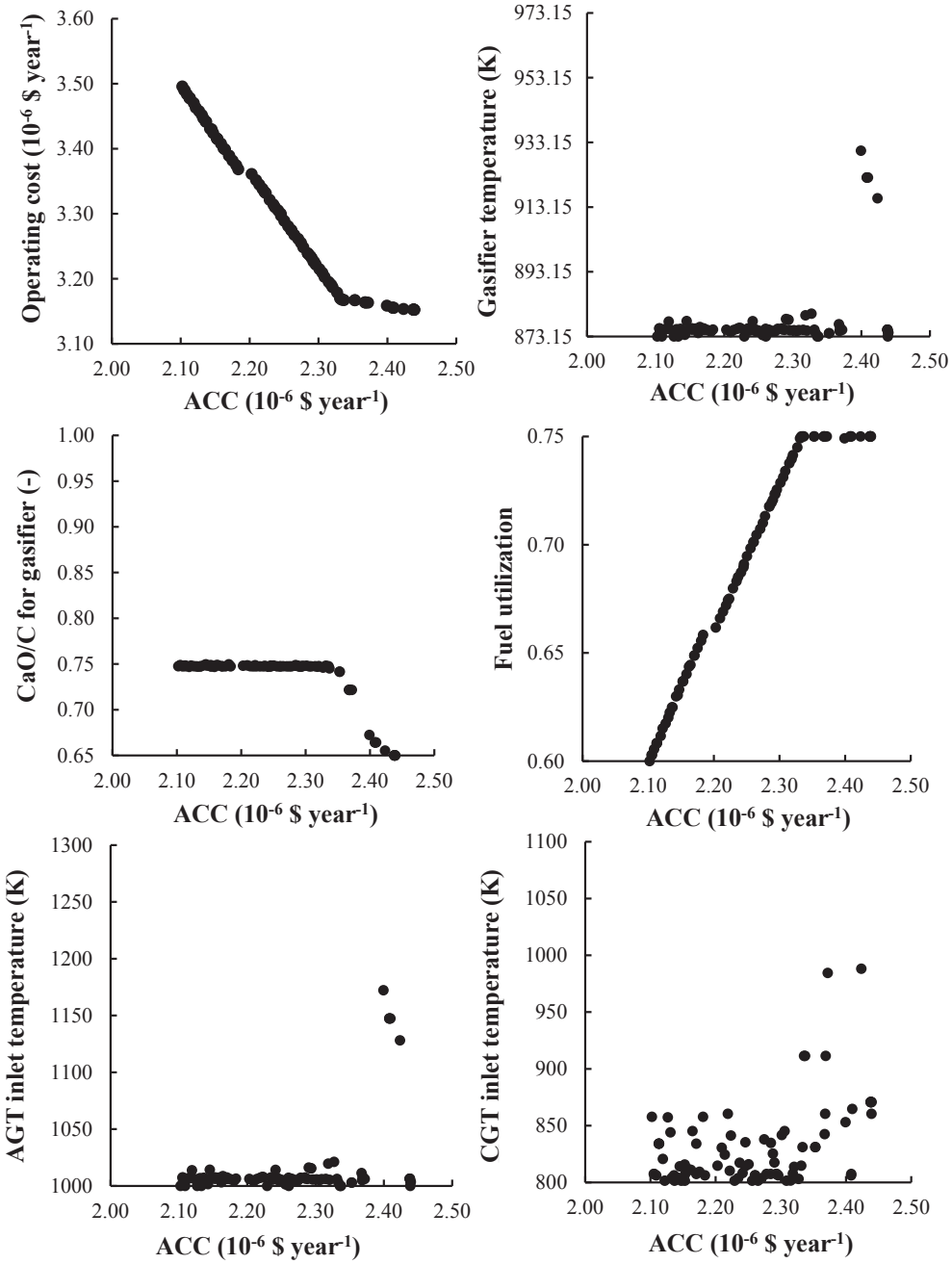

Fig. 9. Optimization results for the integrated SEG-SOFC-GT plant for MOO problem 3.

Table 4
Variations in electricity and annualized capital cost per kWh with plant capacities.

Plant capacity (Wood)	Levelized electricity cost ($ kWh^{-1})		Annualized capital cost per kWh ($ kWh^{-1}year^{-1})	
	This study	Reference [23]	This study	Reference [23]
1.6 MM	0.1114	0.1547	0.0707	0.0714
4.8 MW	0.0845	0.1313	0.0437	0.0506
8 MW	0.0772	0.1298	0.0365	0.0477

electricity cost (W_1 = 0.25), Pareto solution with higher levelized electricity cost is chosen by NFM. Finally, GRA method recommends Pareto solution with lower value of levelized electricity cost compared to the recommended optimal solutions by NFM using three different weights.

6.2. Parametric uncertainty analysis

It is always important to choose and implement robust solution in the industrial practice. Parametric uncertainty analysis is useful in evaluating the sensitivity of the Pareto solutions. Probability distribution functions can be used to describe the uncertainties in parameters. The performance of the proposed integrated energy plant may be affected by a number of uncertain operating and market parameters. Here, ten relevant uncertain parameters are choosen for analyzing their impacts on the Pareto solutions. For the selected operating and market parameters, probability distribution functions are described in Table 6. Based on previous studies, normal distributions were assumed for interest rest, wood price, oxygen price, electricity price, $CaCO_3$ price and cement price [23], and beta distributions were assumed for yearly operation, gasifier and SOFC life time and life time of other equipment. Finally, uniform distribution was considered for gasifier and SOFC

Table 5
NFM parameters used for the ranking of Pareto solutions found by OSMOSE.

	MOO P1		MOO P2		MOO P3		**MOO P4**	
	Annual Profit ($ year^{-1})	ACC ($ year^{-1})	Exergy Efficiency (%)	ACC ($ year^{-1})	ACC ($ year^{-1})	Operating Cost ($ year^{-1})	LEC ($ kWh^{-1})	ACC per kWh ($ year^{-1} kWh^{-1})
Goal	Max	Min	Max	Min	Min	Min	Min	Min
Min value	6.30×10^6	2.11×10^6	52.6	2.11×10^6	2.10×10^6	3.15×10^6	6.58×10^{-2}	2.77×10^{-2}
Max value	8.30×10^6	2.42×10^6	61.2	2.61×10^6	2.44×10^6	3.50×10^6	7.67×10^{-2}	2.84×10^{-2}
Range	2.00×10^6	3.05×10^5	8.58	4.99×10^5	3.37×10^5	3.44×10^5	1.09×10^{-2}	6.76×10^{-4}
Weights	0.25, 0.50, 0.75	0.25, 0.50, 0.75	0.25, 0.50, 0.75	0.25, 0.50, 0.75	0.25, 0.50, 0.75	0.25, 0.50, 0.75	0.25, 0.50, 0.75	0.25, 0.50, 0.75
Threshold								
Indifference	2.00×10^5	3.05×10^4	0.858	4.99×10^4	3.37×10^4	3.44×10^4	1.09×10^{-3}	6.76×10^{-5}
Preference	4.00×10^5	6.10×10^4	1.72	9.98×10^4	6.74×10^4	6.87×10^4	2.18×10^{-3}	1.35×10^{-4}
Veto	1.60×10^5	2.44×10^4	6.87	3.99×10^5	2.70×10^5	2.75×10^5	8.71×10^{-3}	5.40×10^{-4}

capital cost factor.

The parametric uncertainty analysis methodology for the Pareto solutions can be found in literature [23,24,26]. In the parametric uncertainty analysis, 500 economic scenarios were generated, using distribution functions of uncertain parameters, and then best and top five optimal solutions were identified. For easier presentation of uncertainty analysis results, only 15 Pareto solutions representing all regions of the Pareto front were chosen for each optimization problem (MOO problem 1–4). The chosen optimal solutions for parametric uncertainty analysis are numbered from 1 to 15, as shown in Fig. 11(a)–(d).

For MOO problem 1, Fig. 12 presents ranking of the Pareto solutions, using 500 economic scenarios. These solutions are ranked based on two different percentages: best solution and one of the top five solutions, for 500 economic scenarios. For 215 economic scenarios (43% of 500), Pareto solution 10 is the best solution, because this solution has minimum value of absolute relative change in the annual profit. Further, Pareto solutions 10 and 12–15 are in top five solutions for more than 8% economic scenarios. This parametric uncertainty analysis suggests that Pareto solution 10 is the least sensitive solution compared to all others solutions, hence it can be chosen by the decision maker as a

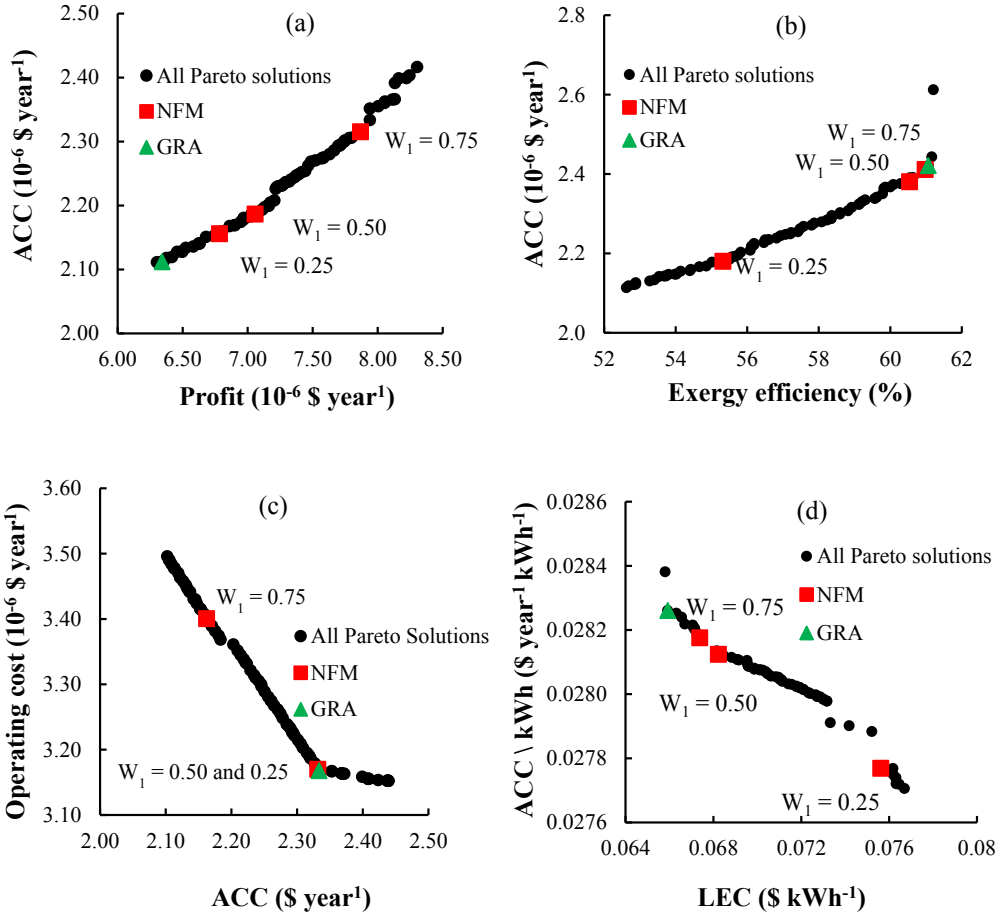

Fig. 10. Selection of Pareto solutions by NFM (3 different weights) and GRA method for the integrated SEG-SOFC-GT plant: (a) MOO problem 1, (b) MOO problem 2, (c) MOO problem 3, and (d) MOO problem 4.

Table 6
Definition of distribution functions for the operating and market parameters [23].

Operating and market parameters	Distribution function	
Yearly operation (YO, h year^{-1})	Beta	c = 8600, α = 3.9, β = 1.2
Interest rate (IR, %)	Normal	μ = 0.06, σ = 0.01
Gasifier and SOFC life time (LT1, year)	Beta	c = 10, α = 5.8, β = 4
Other equipment life time (LT2, year)	Beta	c = 30, α = 5.8, β = 4
Gasifier and SOFC capital cost factor (CCOST, –)	Uniform	a = −0.3, b = 0.3
Electricity price (EP, $ kWh^{-1})	Normal	μ = 0.16, σ = 0.02
Oxygen price (OP, $ (3600 kg)$^{-1}$)	Normal	μ = 235, σ = 50
Wood price (WP, $ (3600 kg)$^{-1}$)	Normal	μ = 360, σ = 50
$CaCO_3$ price (CACO3P, $ (3600 kg)$^{-1}$)	Normal	μ = 88.2, σ = 20
Cement price (CMP, $ (3600 kg)$^{-1}$)	Normal	μ = 270, σ = 50

preferred solution.

For MOO problem 2, Fig. 13 presents ranking of the Pareto solutions, using 500 economic scenarios. These solutions are ranked to identify the best solution and top five good solutions, based on 500 randomly generated economic scenarios. For this optimization problem, Pareto solution 1 is found to be the best solution for 153 economic scenarios (30.6% of 500), based on the minimum absolute relative change in the total capital cost value. For all economic scenarios, Pareto solutions 1–4 are in the top five solutions, with nearly same percentage (more than 9%). Therefore, this parametric uncertainty analysis recommends that Pareto solution 1 for MOO problem 2 is the preferred solution for implementation.

For MOO problem 3, Fig. 14 shows the ranking of the Pareto solutions, using 500 economic scenarios. As mentioned earlier, 15 Pareto solutions found by OSMOSE for MOO problem 3 are considered for parametric uncertainty analysis, to identify one best and five good solutions. Pareto solution 15 has minimum value of absolute relative change in the operating cost, for majority of the generated economic scenarios (356 of 500). For 500 economic scenarios, Pareto solutions 12–15 are in the top five solutions, with nearly same percentage (approximately 16%), and this percentage is much better than the other solutions. Therefore, for MOO problem 3, this parametric uncertainty analysis suggests that solution 15 is the most robust solution.

Finally, ranking of 15 Pareto solutions for MOO problem 4 is shown in Fig. 15. In total, 500 number of economic scenarios were generated using the distribution functions of uncertain parameters. Pareto solution 1 has the minimum value of absolute relative change in the levelized electricity cost, for 56.4% (282 out of 500) economic scenarios. Further, Pareto solutions 1–4 are in the top five solutions, with percentage more than 11%. Based on this parametric uncertainty analysis for MOO problem 4, decision maker can chose Pareto solution 1 for the practical implementation.

7. Conclusions

In this work, thermo-economic performance of the sorption enhanced steam biomass gasification (SEG) with solid oxide fuel cell, for the production of power and heat from Eucalyptus wood chips, was investigated using multi-objective optimization approach. The plant model was

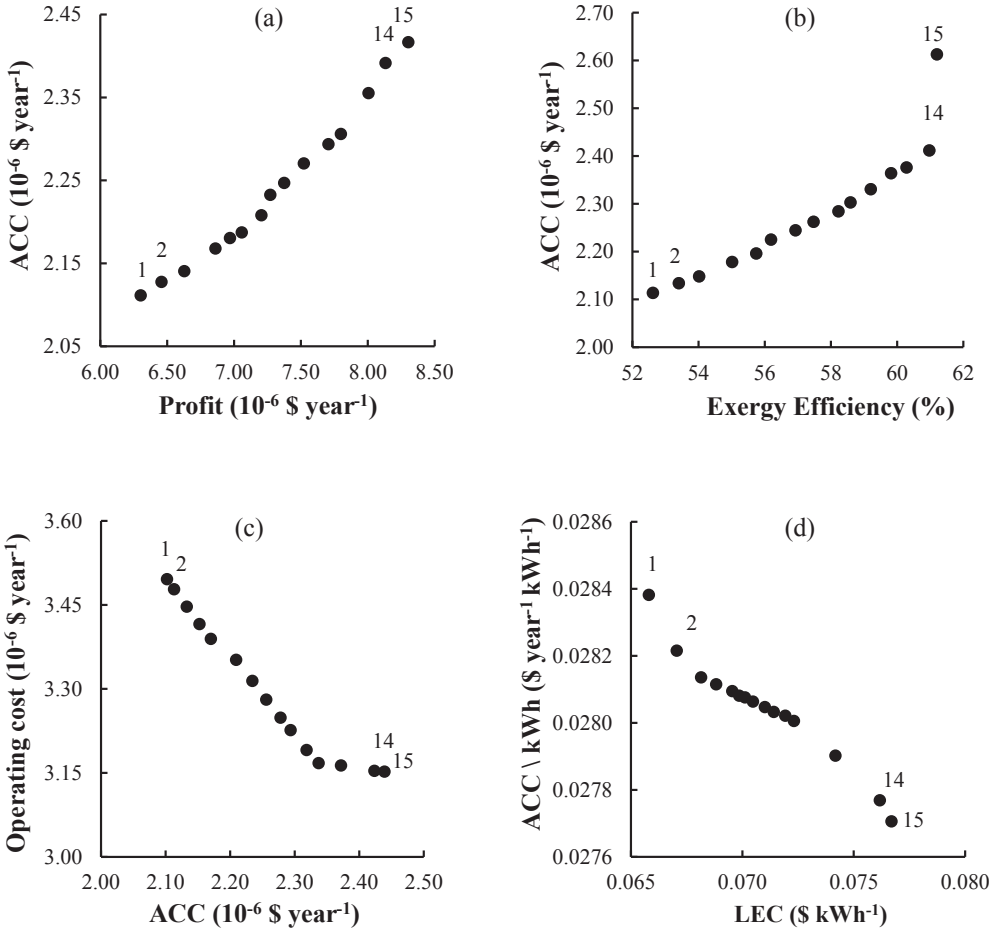

Fig. 11. Pareto solutions selected for parametric uncertainty analysis of the integrated SEG-SOFC-GT plant. (a) MOO problem 1, (b) MOO problem 2, (c) MOO problem 3, and (d) MOO problem 4.

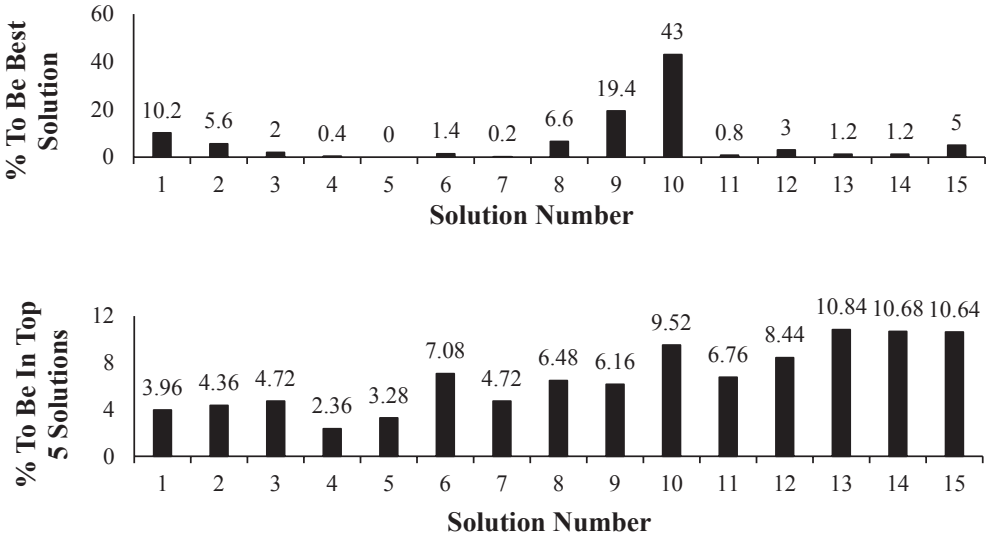

Fig. 12. Parametric uncertainty analysis results for MOO P1 (integrated SEG-SOFC-GT plant).

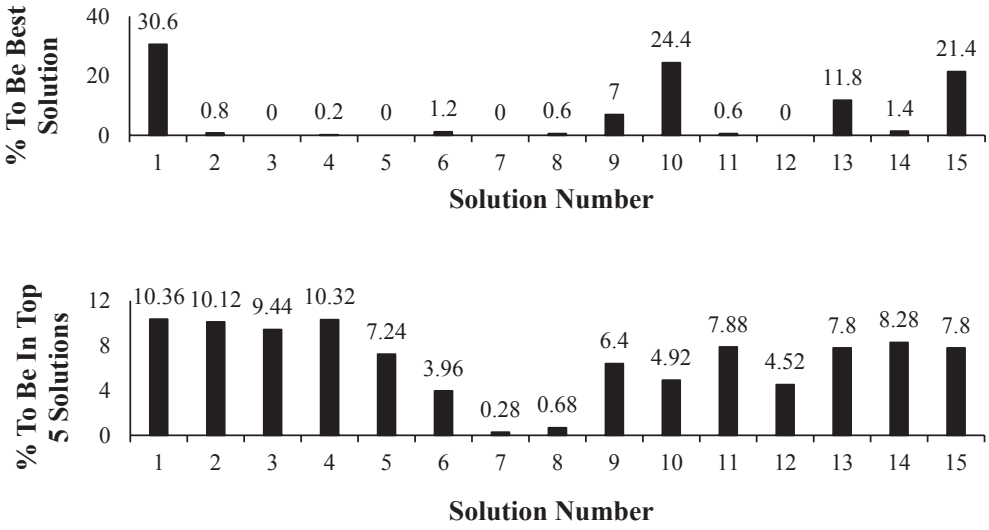

Fig. 13. Parametric uncertainty analysis results for MOO P2 (integrated SEG-SOFC-GT plant).

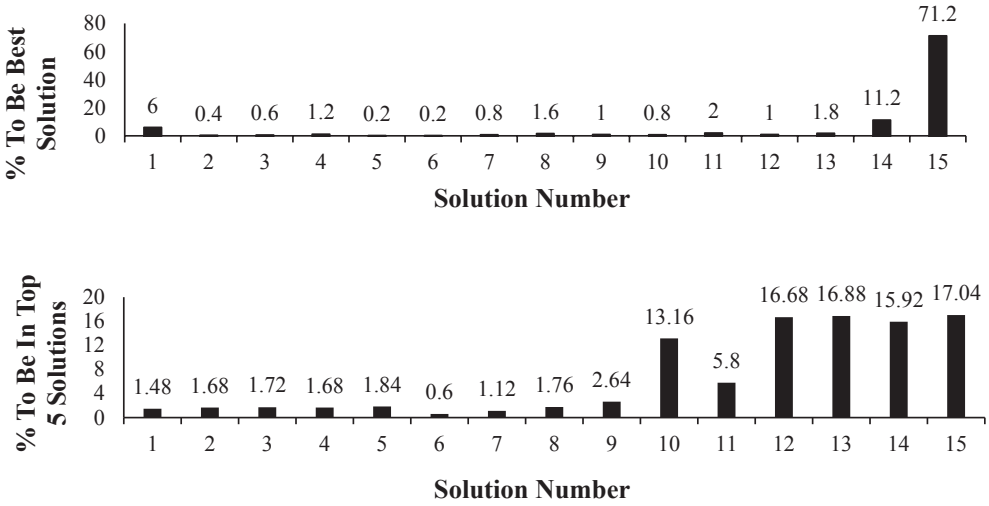

Fig. 14. Parametric uncertainty analysis results for MOO P3 (integrated SEG-SOFC-GT plant).

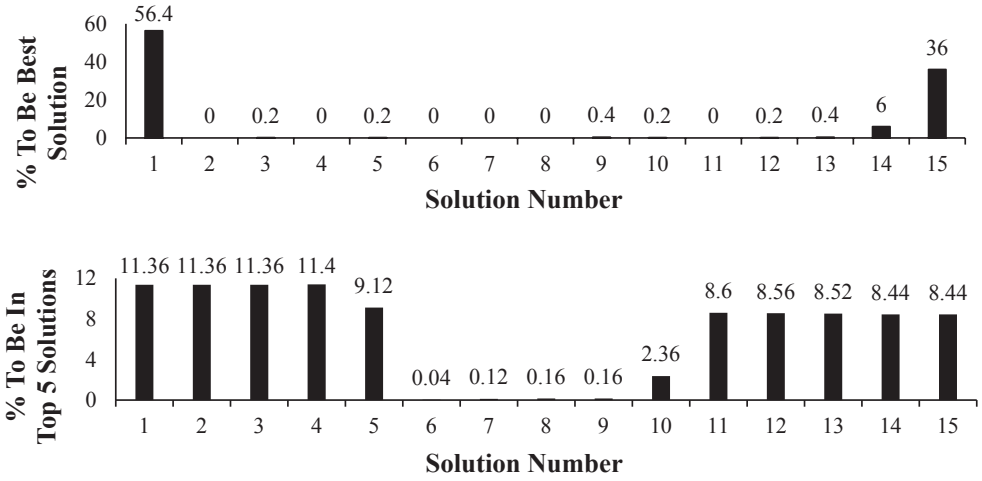

Fig. 15. Parametric uncertainty analysis results for MOO P4 (integrated SEG-SOFC-GT plant).

developed in Aspen Plus simulator, which includes SEG, CaO looping, hot gas cleaning, steam reforming, SOFC-GT, catalytic burning, CO_2 compression and cement production. In total, four relevant bi-objective optimization problems, considering different performance criteria, were studied to understand the performance of integrated energy plant. The proposed plant shows better heat integration among gasifier, catalytic burner and rotary kiln, and also has high thermodynamic performance (maximum exergy efficiency = 61.2%). The Pareto solutions found for different MOO problems were ranked using net flow method and gray relational analysis method to recommend suitable plant design for implementation. Notably, Pareto solutions recommended by both the ranking methods were always different. Finally, to study the effect of uncertain market and operating parameters on the performance of the plant, parametric uncertainty analysis was performed to recognize robust Pareto solutions, for each MOO problem. A distinct plant design is represented by each Pareto solution, and the parametric uncertainty analysis identifies the best and five good designs.

Declaration of interest

The authors declare that they have no known competing financial interests or personal relationships that could have appeared to influence the work reported in this paper.

Acknowledgments

Support from The Royal Golden Jubilee Ph.D. Program (The Thailand Research Fund) and Chulalongkorn Academic Advancement into Its 2nd Century Project is gratefully acknowledged. A. Arpornwichanop would also thank the financial support provided by the “Research Chair Grant”, National Science and Technology Development Agency (NSTDA).

References

[1] Moreira JR. Global biomass energy potential. Mitig Adapt Strat Glob Change 2006;11(2):313–42.
[2] Demirbaş A. Biomass resource facilities and biomass conversion processing for fuels and chemicals. Energy Convers Manage 2001;42(11):1357–78.
[3] Celebi AD, Ensinas AV, Sharma S, Maréchal F. Early-stage decision making approach for the selection of optimally integrated biorefinery processes. Energy 2017;137:908–16.
[4] Basu P. Biomass gasification, pyrolysis and torrefaction. 2nd ed. Burlington: Academic Press; 2013.
[5] Gholamian E, Zare V, Mousavi SM. Integration of biomass gasification with a solid oxide fuel cell in a combined cooling, heating and power system: a thermodynamic and environmental analysis. Int J Hydrogen Energy 2016;41(44):20396–406.
[6] Udomsirichakorn J, Salam PA. Review of hydrogen-enriched gas production from steam gasification of biomass: the prospect of CaO-based chemical looping gasification. Renew Sustain Energy Rev 2014;30:565–79.
[7] Florin NH, Harris AT. Hydrogen production from biomass coupled with carbon dioxide capture: the implications of thermodynamic equilibrium. Int J Hydrogen Energy 2007;32(17):4119–34.
[8] Shiyi C, Wang D, Xue Z, Sun X, Xiang W. Calcium looping gasification for high-concentration hydrogen production with CO_2 capture in a novel compact fluidized bed: simulation and operation requirements. Int J Hydrogen Energy 2011;36(8):4887–99.
[9] Detchusananard T, Im-orb K, Ponpesh P, Arpornwichanop A. Biomass gasification integrated with CO_2 capture processes for high-purity hydrogen production: process performance and energy analysis. Energy Convers Manage 2018;171:1560–72.
[10] Udomsirichakorn J, Basu P, Salam PA, Acharya B. CaO-based chemical looping gasification of biomass for hydrogen-enriched gas production with in situ CO_2 capture and tar reduction. Fuel Process Technol 2014;127:7–12.
[11] Sucipta M, Kimijima S, Suzuki K. Performance analysis of the SOFC – MGT hybrid system with gasified biomass fuel. J Power Sources 2007;174(1):124–35.
[12] Gadsbøll R, Thomsen J, Bang-Møller C, Ahrenfeldt J, Henriksen UB. Solid oxide fuel cells powered by biomass gasification for high efficiency power generation. Energy 2017;131:198–206.
[13] Colpan CO, Hamdullahpur F, Dincer I, Yoo Y. Effect of gasification agent on the performance of solid oxide fuel cell and biomass gasification systems. Int J Hydrogen Energy 2010;35(10):5001–9.
[14] Bang-Møller C, Rokni M, Elmegaard B. Exergy analysis and optimization of a biomass gasification, solid oxide fuel cell and micro gas turbine hybrid system. Energy 2011;36(8):4740–52.
[15] Recalde M, Woudstra T, Aravind AV. Renewed sanitation technology: a highly efficient faecal-sludge gasification–solid oxide fuel cell power plant. Appl Energy 2018;222:515–29.
[16] Rangaiah GP, Sharma S, Sreepathi BK. Multi-objective optimization for the design and operation of energy efficient chemical processes and power generation. Curr Opin Chem Eng 2015;10:49–62.
[17] Sharma S, Rangaiah GP. Multi-objective optimization applications in chemical engineering. In: Rangaiah GP, Bonilla-Petriciolet A, editors. Multi-objective optimization in chemical engineering: developments and applications. Wiley; 2013.
[18] Abdollahi G, Meratizaman M. Multi-objective approach in thermoenvironomic optimization of a small-scale distributed CCHP system with risk analysis. Energy Build 2011;43(11):3144–53.
[19] Quddus MR, Zhang Y, Ray AK. Multi-objective optimization in solid oxide fuel cell for oxidative coupling of methane. Chem Eng J 2010;165(2):639–48.
[20] Jokar MA, Ahmadi MH, Meyer JP, Pourfayaz F, Ming T. Thermodynamic evaluation and multi-objective optimization of molten carbonate fuel cell-supercritical CO_2 Brayton cycle hybrid system. Energy Convers Manage 2017;153:538–56.
[21] Sadeghi M, Mehr AS, Zar M, Santarelli M. Multi-objective optimization of a novel syngas fed SOFC power plant using a downdraft gasifier. Energy 2018;148:16–31.
[22] Caliandro P, Tock L, Ensinas A, Maréchal F. Thermo-economic optimization of a Solid Oxide Fuel Cell – Gas turbine system fuelled with gasified lignocellulosic biomass. Energy Convers Manage 2014;85:764–73.
[23] Sharma S, Celebi AD, Maréchal F. Robust multi-objective optimization of gasifier and solid oxide fuel cell plant for electricity production using wood. Energy 2017;137:811–22.
[24] Sharma S, Maréchal F. Robust multi-objective optimization of solid oxide fuel cell–gas turbine hybrid cycle and uncertainty analysis. J Electrochem Energy Convers Storage 2018:15(4).
[25] Wang Z, Rangaiah GP. Application and analysis of methods for selecting an optimal solution from the Pareto-optimal front obtained by multiobjective optimization. Ind Eng Chem Res 2017;56(2):560–74.
[26] Tock L, Maréchal F. Decision support for ranking Pareto optimal process designs under uncertain market conditions. Comput Chem Eng 2015;83:165–75.
[27] Ladpala S, Ketjoy N, Rakwichian W, Intanon P. Performance evaluation of a 25 kW_e biomass power generation system prototype for community in Thailand. Int J

Renew Energy 2007;2(2).
[28] Li XT, Grace JR, Lim CJ, Watkinson AP, Chen HP, Kim JR. Biomass gasifcation in a circulating fluidized bed. Biomass Bioenergy 2004;26(2):171–93.
[29] Pfeifer C, Puchner B, Hofbauer H. Comparison of dual fluidized bed steam gasification of biomass with and without selective transport of CO_2. Chem Eng Sci 2009;64(23):5073–83.
[30] Soukup G, Pfeifer C, Kreuzeder A, Hofbauer H. In Situ CO_2 Capture in a Dual Fluidized Bed Biomass Steam Gasifier – Bed Material and Fuel Variation. Chem Eng Technol 2009;32(3):348–54.
[31] Doherty W, Reynolds A, Kennedy D. The effect of air preheating in a biomass CFB gasifier using ASPEN Plus simulation. Biomass Bioenergy 2009;33(9):1158–67.
[32] Facchinetti E. Integrated solid oxide fuel cell – gas turbine hybrid systems with or without CO_2 separation [dissertation]. Switzerland: École Polytechnique Fédérale de Lausanne; 2012.
[33] Yoobanpot N, Jamsawang P, Horpibulsuk S. Strength behavior and microstructural characteristics of soft clay stabilized with cement kiln dust and fly ash residue. Appl Clay Sci 2017;141:146–56.
[34] Kääntee U, Zevenhoven R, Backman R, Hupa M. Cement manufacturing using alternative fuels and the advantages of process modelling. Fuel Process Technol 2004;85(4):293–301.
[35] Aranda-Usón A, López-Sabirón AM, Ferreira G, Llera-Sastresa E. Uses of alternative fuels and raw materials in the cement industry as sustainable waste management options. Renew Sustain Energy Rev 2013;23:242–60.
[36] Rodriguez N, Murillo R, Abanades JC. CO_2 capture from cement plants using oxyfired precalcination and/or calcium looping. Environ Sci Technol 2012;46(4):2460–6.
[37] Johnsen K, Grace JR, Elnashaie SSEH, Kolbeinsen L, Eriksen D. Modeling of sorption-enhanced steam reforming in a dual fluidized bubbling bed reactor. Ind Eng Chem Res 2006;45(12):4133–44.
[38] Cormos A-M, Dinca C, Cormos C-C. Multi-fuel multi-product operation of IGCC power plants with carbon capture and storage (CCS). Appl Therm Eng 2015;74:20–7.
[39] Patcharavorachot Y, Arpornwichanop A, Chuachuensuk A. Electrochemical study of a planar solid oxide fuel cell: role of support structures. J Power Sources 2008;177(2):254–61.
[40] Van Herle J, Maréchal F, Leuenberger S, Favrat D. Energy balance model of a SOFC cogenerator operated with biogas. J Power Sources 2004;26(2):171–93.
[41] Manatura K, Lu J-H, Wu K-T, Hsu H-T. Exergy analysis on torrefied rice husk pellet in fluidized bed gasification. Appl Therm Eng 2017;111:1016–24.
[42] Parvez AM, Mujtaba IM, Wu T. Energy, exergy and environmental analyses of conventional, steam and CO_2-enhanced rice straw gasification. Energy 2016;94:579–88.
[43] El-Emam RS, Dincer I, Naterer GF. Energy and exergy analyses of an integrated SOFC and coal gasification system. Int J Hydrogen Energy 2012;37(2):1689–97.
[44] Szargut J, Morris DR, Stewart FR. Exergy analysis of thermal, chemical, and metallurgical processes. Hemisphere Publish Corpor 1998.
[45] Zhang X, Li H, Liu L, Bai C, Wang S, Song S, et al. Exergetic and exergoeconomic assessment of a novel CHP system integrating biomass partial gasification with ground source heat pump. Energy Convers Manage 2018;156:666–79.
[46] Cohce MK, Dincer I, Rosen MA. Energy and exergy analyses of a biomass-based hydrogen production system. Bioresour Technol 2011;102(18):8466–74.
[47] Deb K. Multi-objective optimization using evolutionary algorithm. Chichester: Chichester; 2001.
[48] Sharma S, Lim ZC, Rangaiah GP. Process design for economic, environmental and safety objectives with an application to cumene process. In: Rangaiah GP, Bonilla-Petriciolet A, editors. Multi-Objective Optimization in Chemical Engineering: Developments and Applications. Wiley; 2013.
[49] Maréchal F, Palazzi F, Godat J, Favrat D. Thermo-economic modelling and optimization of fuel cell systems. Fuel Cells 2004;5(1):5–24.
[50] Pelster S. Environomic modeling and optimization of advanced combined cycle cogeneration power plants including CO_2 separation options. EPFL Thesis 1998:89–90.
[51] Ulrich GD, Vasudevan PT. Chemical engineering process design & economics: a practical guide. 2nd ed. Taylor & Francis Inc; 2004.
[52] Turton R, Bailie RC, Whiting WB, Shaeiwitz JA. Analysis, synthesis and design of chemical processes. 4th ed. Prentice Hall; 2012.
[53] Cormos C-C. Economic implications of pre- and post-combustion calcium looping configurations applied to gasification power plants. Int J Hydrogen Energy 2014;39(20):10507–16.
[54] Alyasri SAAH, Alkroosh IS, Sarker PK. Feasibility of producing nano cement in a traditional cement factory in Iraq. Case Stud Constr Mater 2017;7:91–101.
[55] Lee ESQ, Rangaiah GP. Optimization of recovery processes for multiple economic and environmental objectives. Ind Eng Chem Res 2009;48(16):7662–81.
[56] Sharma S, Rangaiah GP. Modeling and optimization of a fermentation process integrated with cell recycling and pervaporation for multiple objectives. Ind Eng Chem Res 2012;51(15):5542–51.